Available online at www.sciencedirect.com
ScienceDirect
Comput. Methods Appl. Mech. Engrg. 196 (2007) 4250–4271
Computer methods in applied mechanics and engineering
www.elsevier.com/locate/cma

Stochastic simulation of riser-sections with uncertain measured pressure loads and/or uncertain material properties

Jasmine Foo [a], Zohar Yosibash [b,*], George Em Karniadakis [a]

[a] Division of Applied Mathematics, Brown University, Providence, RI, USA
[b] Pearlstone Center for Aeronautical Engineering Studies, Department of Mechanical Engineering, Ben-Gurion University, Beer-Sheva, Israel

Received 17 October 2005; received in revised form 11 January 2007; accepted 25 April 2007
Available online 10 May 2007

Abstract

We investigate three-dimensional problems in solid mechanics with stochastic loading or material properties. To solve these problems, we use a spectral expansion of the solution and random inputs based on Askey-type orthogonal polynomials in terms of independent, identically distributed (i.i.d) random variables. A Galerkin procedure using these types of expansions, the generalized Polynomial Chaos (gPC) method, is employed to solve linear elasticity problems. An analagous spectral collocation formulation is used to study problems in nonlinear elasticity. These methods both cast the stochastic problem as a coupled or decoupled high-dimensional system of deterministic PDEs, which is then solved numerically using a deterministic p-finite element solver. We present algorithms for solving certain coupled systems arising from the stochastic Galerkin projection without modifying the original deterministic solver. Three-dimensional riser-sections undergoing elastic deformations due to random pressure loads are considered. We also model a riser-section with stochastic Young's modulus undergoing deterministic loads. It is demonstrated that the gPC method provides accurate and efficient results at a speed-up factor of two and three orders of magnitude compared to traditional Monte-Carlo simulations. For nonlinear problems, the stochastic collocation method is also shown to be much faster than Monte-Carlo simulation, while still rivaling this method in simplicity of implementation.

Keywords: Uncertainty quantification; Karhunen–Loève (K–L) expansion; p-FEM; Polynomial chaos; Random fluid loads; Stochastic collocation

1. Introduction

The study of the mechanical response of structures with stochastic loading or material properties has many applications in engineering. The stochastic nature of physical quantities may come from an uncertainty in measurements or insufficient information. For example, modeling the Young's modulus of a material as a random variable can account for ignorance of its true value. Alternatively, the parameters in a problem may possess an intrinsic randomness. External loading on structures from environmental sources such as fluid flow is often modeled as a temporal or spatio-temporal stochastic process. For example, in [1], noisy ocean wave-induced forces on offshore structures are modeled as a Gaussian random process in time. In addition, material properties of a structure may vary from point to point in the material; thus they can be represented as spatial random processes. Much of the work in this field (e.g. [2]) has been based on the assumption that the Young's modulus is random and the Poisson ratio is deterministic. There has, however, been some work such as [3] where both quantities are considered as spatial random processes. In [4], the generalized Polynomial Chaos (gPC) method using Hermite polynomials was applied to study 3-D elasto-plastic bodies with uncertain material properties. Although only four terms in the K–L expansion are used in [4] with low-order finite elements, the authors demonstrate the accuracy and efficiency when computing the

* Corresponding author. Tel.: +972 8 6477103; fax: +972 8 6477101.
E-mail addresses: jfoo@dam.brown.edu (J. Foo), zohary@bgu.ac.il (Z. Yosibash), gk@dam.brown.edu (G.E. Karniadakis).

0045-7825/$ - see front matter © 2007 Elsevier B.V. All rights reserved.
doi:10.1016/j.cma.2007.04.005

mean and standard deviation by PC compared to Monte-Carlo (MC) simulation.

In both situations with inherent stochasticity as well as uncertainty in measurements, modeling these systems with their deterministic means may lead to unrealistically conservative solutions. The moment statistics of a solution carry important information regarding the presence and probability of extreme events that might lead to catastrophic failures. However, Monte-Carlo simulations for the stochastic analysis of such complex systems are often computationally prohibitive. In this paper we apply alternative numerical methods to approximate stochastic solutions to these types of problems. Our primary motivation is to apply and evaluate the viability of the *stochastic Galerkin* and *collocation* methods in three-dimensional elasticity problems with non-trivial geometries and stochastic loading or material properties. These model problems are inspired from the physical scenario of marine risers with uncertain material properties undergoing a noisy ocean cross-flow. Various riser-section structures are considered with mean pressure loading profiles based upon experimental data of fluid flow past a circular cylinder. The stochastic quantities include the magnitude of the pressures (modeled as a spatial random process) and the material properties (modeled as a random variable). In order to evaluate the viability of these methods we consider mainly the computational costs, accuracy of the solution and the ease of implementation. In addition, we formulate an algorithm to easily implement the stochastic Galerkin method in certain cases, which acts as a wrapper code around the deterministic solver. Various types of problems are tested, including those that are linear/nonlinear in physical space and linear/nonlinear in random space. It is, thus, our aim to provide the reader with some experimental analysis of the suitability of these methods to various types of three-dimensional problems, with regard to the accuracy and computational costs involved. In addition, we would like to provide sufficiently general algorithms and formulations for easily implementing these techniques.

The stochastic spectral methods used herein employ spectral expansions of the solution and random inputs based on Askey-type orthogonal polynomials in terms of independent, identically distributed random variables. These types of expansions are called generalized Polynomial Chaos (gPC) expansions and were first introduced in [5] as a generalization of the Hermite Chaos expansions originally proposed by Wiener [6]. Once equipped with these spectral expansions in random space, one can formulate stochastic Galerkin and collocation spectral methods using the usual projections. The stochastic Galerkin method, usually called the generalized Polynomial Chaos (gPC) method, transforms the original problem into a set of coupled deterministic problems to be solved by standard finite element methods (FEMs) [5,7–10]. In some cases, when the problem is linear in random space (e.g., stochastic loading for linear elasticity), the resulting deterministic system of equations is decoupled and, thus, much less computationally intensive. In these cases, rewriting of the deterministic solver is not necessary. However, in the case of nonlinearities in random space (e.g., stochastic material properties), this method usually requires extensive rewriting of the deterministic solver, a distinction that makes the gPC method less attractive than the collocation method. The stochastic collocation method [11] is "blind" to nonlinearities in random space and hence easier to implement than gPC in problems with random nonlinearities. As in deterministic spectral methods, the stochastic collocation procedure involves specifying a set of collocation points, usually chosen to coincide with a specific cubature rule. In this paper we briefly address the issue of sparse grid quadrature, where a sparse rather than full set of quadrature points is used, with a corresponding modification to the cubature weights and rule. This technique significantly reduces computational costs, which compound with increasing dimensionality in random space.

Both the gPC and stochastic collocation methods can lead to considerable speed-up in computational time as compared to MC simulation. It should be noted, however, that in problems with a large number of random dimensions, the computational cost of MC scales better than these methods. In this work we consider problems with relatively low random dimensionality, thus restricting ourselves to the realm in which the stochastic spectral methods are competitive with MC. The random inputs are either random variables or processes represented by a truncated Karhunen–Loève (K–L) expansion, which is a representation of a random process in terms of a linear sum of uncorrelated random variables [7].

The paper is structured as follows. In Section 2, we present the notation and two model structures representing risers: a thin-walled elastic tube with and without a spherical reinforcement. We also provide there a description of the experimental fluid loads and material properties upon which random inputs are modeled in the paper. In Section 3, the basics of the generalized Polynomial Chaos are presented, along with the general formulation for the stochastic Galerkin and collocation methods. In Section 4, the Karhunen–Loève expansion for second-order random process inputs is described. The stochastic Galerkin and collocation schemes for linear and nonlinear elasticity systems are presented in Section 5. There we address various cases of stochastic inputs for both methods, including the coupled gPC scheme for the linear elasticity system with stochastic material properties. A solution algorithm by the iterative Gauss–Seidel method is provided for the special case of stochastic Young's modulus and deterministic Poisson ratio. In Section 6, we provide a description of the specific random process loading, which will be used in the numerical examples (Section 7). We also investigate several cases, including linear elasticity problems using the gPC method and linear/nonlinear elasticity problems using the stochastic collocation method for both stochastic loading and material properties. We perform numerical experiments to investigate the influence of the finite element

space-discretization errors on the results, as well as the effect of using sparse grid collocation. We conclude in Section 8 with a brief summary.

2. Preliminaries

2.1. Deterministic linear and nonlinear elasticity

Consider three-dimensional domains $\mathscr{D} \subset \mathbb{R}^3$, in which every point is represented by Cartesian coordinates $\boldsymbol{x} = (x_1, x_2, x_3)^{\mathrm{T}}$. We denote the displacement vector at point $\boldsymbol{x}$ by $\boldsymbol{u}(\boldsymbol{x}) = (u_1(\boldsymbol{x}), u_2(\boldsymbol{x}), u_3(\boldsymbol{x}))^{\mathrm{T}}$, and the body forces by $\boldsymbol{f}(\boldsymbol{x})$. The second-order strain tensor under the assumption of small strains is defined to be

$$\varepsilon_{ij} \stackrel{\text{def}}{=} \frac{1}{2}\left(\frac{\partial u_i}{\partial x_j} + \frac{\partial u_j}{\partial x_i}\right), \quad i,j = 1,2,3, \tag{1}$$

whereas the second-order Almansi strain tensor is used for nonlinear elasticity when geometric nonlinearity (large displacements) is addressed

$$e_{ij} \stackrel{\text{def}}{=} \frac{1}{2}\left(\frac{\partial u_i}{\partial x_j} + \frac{\partial u_j}{\partial x_i} - \sum_{k=1}^{3} \frac{\partial u_k}{\partial x_i}\frac{\partial u_k}{\partial x_j}\right), \quad i,j = 1,2,3. \tag{2}$$

We restrict our attention to isotropic materials, for which the constitutive relation between strains and stresses is linear (i.e. Hooke's law [12]), determined by two material parameters λ and μ (known as the Lamé constants). In the engineering community the Young's modulus E and the Poisson ratio ν are used, and these are related to Lamé constants

$$E = \frac{\mu(3\lambda + 2\mu)}{\lambda + \mu}, \quad \nu = \frac{\lambda}{2(\lambda + \mu)}. \tag{3}$$

Therefore, if either E or ν are random processes, then both λ and μ are also random processes.

When geometric nonlinearities are considered the Cauchy stress tensor and the Almansi strain tensor are associated via Hooke's law

$$\begin{aligned} \sigma_{ij} &= \sum_{k,l=1}^{3} C_{ijkl} e_{kl}, \quad i,j,k,l = 1,2,3, \\ C_{ijkl} &= \lambda \delta_{ij}\delta_{kl} + \mu(\delta_{ik}\delta_{jl} + \delta_{il}\delta_{jk}), \end{aligned} \tag{4}$$

where δ_{ij} is the Kronecker symbol. In the case of linear elasticity (small displacements), Eq. (4) still holds with ε_{kl} instead of e_{kl}.

Under the assumption of small displacements, one may substitute the kinematic condition into Hooke's law, and by satisfying the equilibrium equations a second-order linear elliptic system of PDEs, named the Navier–Lamé equations, is obtained (see e.g. [12]):

$$-\mu\nabla^2\boldsymbol{u}(\boldsymbol{x}) - (\lambda + \mu)\nabla(\nabla \cdot \boldsymbol{u}(\boldsymbol{x})) = \boldsymbol{f}(\boldsymbol{x}) \quad \text{in } \mathscr{D}. \tag{5}$$

This system is presented here in terms of the Lamé constants for mathematical simplicity. However, from now on we will switch to the more commonly used E and ν. The Navier–Lamé system is complemented by the boundary conditions:

$$T_j \stackrel{\text{def}}{=} \sigma_{ij} n_j = \hat{T}_j, \quad j = 1,2,3 \quad \text{on } \partial\Gamma_T, \tag{6}$$

$$u_j = \hat{u}_j, \quad j = 1,2,3 \quad \text{on } \partial\Gamma_u, \tag{7}$$

where $\hat{\bullet}$ are prescribed functions on the boundary of the domain. If either the body forces $\boldsymbol{f}$ or the tractions $\boldsymbol{T}$ are uncertain, then additive uncertainty arises. If the material properties E or ν are uncertain, then multiplicative uncertainty arises.

The weak formulation associated with (5) is (see [13]):

Find $\boldsymbol{u} \in \overset{\circ}{\mathscr{E}}(\mathscr{D})$ so that

$$\mathscr{B}(\boldsymbol{u}, \boldsymbol{v}) = \mathscr{F}^{\mathrm{BF}}(\boldsymbol{v}) + \mathscr{F}^{\mathrm{T}}(\boldsymbol{v}) \quad \forall \boldsymbol{v} \in \overset{\circ}{\mathscr{E}}(\mathscr{D}), \tag{8}$$

where $\overset{\circ}{\mathscr{E}}(\mathscr{D})$ is the space of statically admissible displacement functions, $\mathscr{B}(\boldsymbol{u}, \boldsymbol{v})$ is the elasticity bilinear form defined as

$$\mathscr{B}(\boldsymbol{u}, \boldsymbol{v}) \stackrel{\text{def}}{=} \frac{1}{4}\int_{\mathscr{D}} \sum_{ijkl=1}^{3} C_{ijkl}\left(\frac{\partial u_i}{\partial x_j} + \frac{\partial u_j}{\partial x_i}\right)\left(\frac{\partial v_k}{\partial x_l} + \frac{\partial v_l}{\partial x_k}\right) \mathrm{d}\mathscr{D} \tag{9}$$

and $\mathscr{F}^{\mathrm{BF}}(\boldsymbol{v})$, $\mathscr{F}^{\mathrm{T}}(\boldsymbol{v})$ are the linear forms associated with the body forces and tractions

$$\mathscr{F}^{\mathrm{BF}}(\boldsymbol{v}) \stackrel{\text{def}}{=} \int_{\mathscr{D}} \boldsymbol{f} \cdot \boldsymbol{v}\, \mathrm{d}\mathscr{D},$$

$$\mathscr{F}^{\mathrm{T}}(\boldsymbol{v}) \stackrel{\text{def}}{=} \int_{\partial\mathscr{D}_T} \boldsymbol{T} \cdot \boldsymbol{v}\, \mathrm{d}S.$$

In the case of large-deformations (nonlinear elasticity), the weak formulation is stated in the deformed configuration so that $\mathscr{D} = \mathscr{D}(\boldsymbol{u})$, and (8) remains the same, but the bivariate form is defined as follows:

$$\mathscr{B}(\boldsymbol{u}, \boldsymbol{v}) \stackrel{\text{def}}{=} \frac{1}{4}\int_{\mathscr{D}(\boldsymbol{u})} \sum_{ijkl=1}^{3} C_{ijkl}\left(\frac{\partial u_i}{\partial x_j} + \frac{\partial u_j}{\partial x_i} - \sum_{r=1}^{3}\frac{\partial u_r}{\partial x_i}\frac{\partial u_r}{\partial x_j}\right)\left(\frac{\partial v_k}{\partial x_l} + \frac{\partial v_l}{\partial x_k}\right) \mathrm{d}\mathscr{D}. \tag{10}$$

Furthermore, when pressure boundary conditions are applied, i.e. $\boldsymbol{T} = -p\boldsymbol{n}$, where $\boldsymbol{n}$ is the outward normal to the surface and is, of course, solution dependent, then the linear form $\mathscr{F}^{\mathrm{T}}(\boldsymbol{v})$ becomes nonlinear also:

$$\mathscr{F}^{\mathrm{T}}(\boldsymbol{v}) \stackrel{\text{def}}{=} \int_{\partial\mathscr{D}_T(\boldsymbol{u})} -p\boldsymbol{n}(\boldsymbol{u}) \cdot \boldsymbol{v}\, \mathrm{d}S. \tag{11}$$

Due to the nonlinearities presented in the formulation, the solution for $\boldsymbol{u}$ must be obtained by iterations, see for example [14].

2.2. Geometric models and experimental data

In this work we study two thin-walled riser-sections with and without spherical masses attached to their centers. These models are shown in Fig. 1, where the $x_3 \equiv z$ direction is along the cylinder's lengthwise axis. The length of the risers is 10 m, and outer diameter is 0.5 m. The inner diameter of the cylinders used in the numerical examples

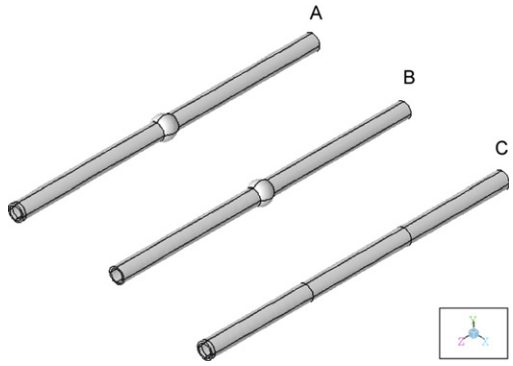

Fig. 1. Geometry and finite element meshes of risers used in the numerical experiments.

vary between 0.4 and 0.48 m. The attached spherical mass has a radius of 0.35 m. In the problems discussed in this paper, the structure is clamped at one end, i.e. $\boldsymbol{u} = 0$ at $z = 10$. Since the intersection of the clamped surface and the inner and outer cylindrical surfaces at $z = 10$ causes stress singularities, the p-finite element mesh contains a refinement in the vicinity of the clamped surface. To investigate the influence of the mesh refinement on the results we also consider for the riser with the sphere reinforcement a coarse mesh. The finite element (FE) meshes A and C in Fig. 1 contain a total of 16 p-FE hexahedral elements, and mesh B contains 12 hexahedral elements.

In an effort to consider a somewhat realistic fluid loading profile, the traction boundary conditions are extracted from experiments performed on a stationary cylinder in a flow field reported in [15]. In this experiment, the mean pressure forces were measured on a circular cylinder in cross-flow, at Reynolds numbers 10^2–10^5, as shown in the right of Fig. 2. In our numerical study of the structural response to a stochastic traction field, we consider the risers to be immersed in water (kinematic viscosity of 10^{-6} m^2/s) flowing at a velocity of 0.5 m/s, thus the flow Re number is $Re = 0.5\ \text{m/s} \times 0.5\ \text{m}/10^{-6}\ \text{m}^2/\text{s} = 2.5 \times 10^5$. The highest experimental C_p profile is at $Re = 2.1 \times 10^5$, considered as a good approximation to the *mean*, and we add a correlated random noise component (to be discussed in more detail in Section 6). The mean value of the C_p profile (according to the lowest curve shown in the right graph of Fig. 2) is approximated with the following seventh-order polynomial:

$$\begin{aligned}(C_p)_{\text{exp}} &= 1.05746 - 0.08684|\theta| - 12.44481|\theta|^2 \\ &\quad + 19.07245|\theta|^3 - 11.92860|\theta|^4 + 3.56530|\theta|^5 \\ &\quad - 0.47547|\theta|^6 + 0.01896|\theta|^7, \quad -\pi \leqslant \theta < \pi\end{aligned} \tag{12}$$

which, in turn, produces the following normal traction (pressure) on the surface of the riser, $T_n = 0.5\rho v^2 C_p$:

$$\begin{aligned}(T_n)_{\text{exp}} &= -125 \times (1.05746 - 0.08684|\theta| - 12.44481|\theta|^2 \\ &\quad + 19.07245|\theta|^3 - 11.92860|\theta|^4 + 3.56530|\theta|^5 \\ &\quad - 0.47547|\theta|^6 + 0.01896|\theta|^7)\ [\text{N/m}^2], \quad -\pi \leqslant \theta < \pi.\end{aligned} \tag{13}$$

Thus, the mean pressure on the riser's surface is described by (13) on the FE model. A view of the x_1–x_2 plane showing the pressure at several distinct points are shown as arrows on the left plot of Fig. 2.

In the numerical examples with uncertain material properties, we use the pressure in (13) to obtain a *deterministic* traction boundary condition.

The characterization of a random Young's modulus is extracted from experimental data in [16]. In the cited work, the Young's modulus of 4140 steel is measured by four different experimental techniques, namely, impulse excitation, nanoindentation, four-point bending and resonant ultrasound spectroscopy. Note that there, each measurement on a sample yielded a different Young's modulus measurement. This may be thought of as uncertainty in measurement; the true value of the Young's modulus is unknown. Thus, we model this quantity as a random variable. We perform a statistical analysis on the experimental data, assuming a prior *uniform* distribution before parameter

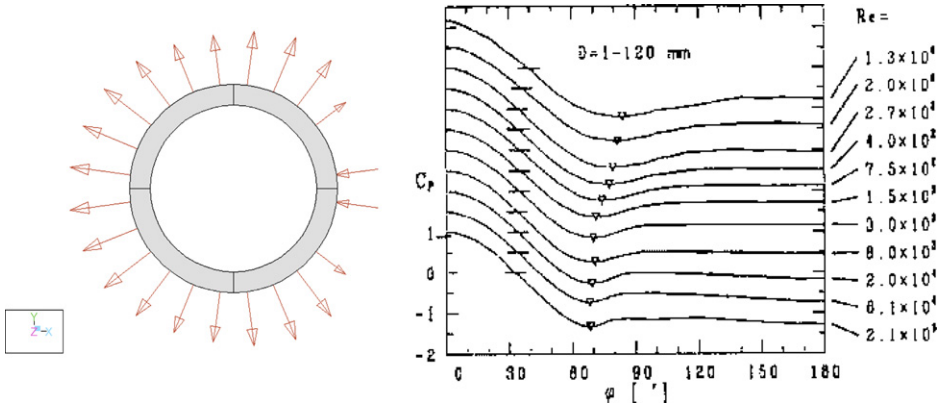

Fig. 2. Pressure boundary conditions from [15] and their application on the riser. Left: cross-sectional view of x_1–x_2 plane. The magnitude and direction of the arrows represent the experimental loading profile (a continuous function is prescribed whereas the arrows represent only its magnitude at a small number of points). Right: reproduction of data from [15], plotting the pressure coefficient as a function of the angle around the cylinder. The lines represent data at different Reynolds numbers.

estimation. Note that there was insufficient data to conclusively confirm a distribution for this analysis. The choice of a uniform distribution is justified as it is the *maximum entropy* distribution for any continuous random variable on an interval of compact support (taken to be the interval between the extreme data points in experimental results). In other words, an assumption of any other prior distribution satisfying the constraints will have smaller entropy, thus containing more information and less uncertainty than the uniform distribution [17,18]. Hence, we model the Young's modulus as a uniformly distributed random variable with mean of 212.74 GPa and standard deviation of 7.26 GPa. The Poisson ratio is taken to be $\nu = 0.3$ in all numerical examples.

3. Stochastic spectral methods

Here a brief overview of the generalized polynomial chaos (gPC) and its properties is provided. Many more details can be found in [7,5]. In addition, we discuss the general model problem and assumptions for which methods in this paper are applicable. Some notations are established and will be used throughout.

3.1. gPC basis

Let us first define a complete probability space $(\Omega, \mathscr{A}, P)$, where Ω is the sample space, P is the probability measure, and $\mathscr{A}$ is the σ-algebra of P-measurable sets. Once again $\mathscr{D} \subset \mathbb{R}^3$ represents the physical domain.

Let $\{\xi_i\}_{i=1}^{\infty}$ be independent, identically distributed continuous random variables mapping $(\Omega, \mathscr{F}) \to (\mathbb{R}, \mathscr{B})$ where $\mathscr{B}$ is the Borel σ-algebra on the reals. The generalized polynomial chaos (gPC) basis is a set of polynomial functionals in terms of the random variables ξ_i. The original polynomial chaos basis was first proposed by Wiener [6] and employed Hermite polynomials in terms of Gaussian random variables. The idea was then generalized to the Askey polynomial scheme and non-Gaussian variables by Xiu and Karniadakis in [5]. Any second-order random process $X(\omega) \in L_2(\Omega, \mathscr{A}, P)$ can be written as a series expansion of gPC basis functions:

$$X(\omega) = a_0 \Phi_0 + \sum_{i_1=1}^{\infty} a_{i_1} \Phi_1(\xi_{i_1}(\omega)) + \sum_{i_1=1}^{\infty} \sum_{i_2=1}^{i_1} a_{i_1 i_2} \Phi_2(\xi_{i_1}(\omega), \xi_{i_2}(\omega)) + \cdots, \tag{14}$$

where $\Phi_n(\xi_{i_1}, \ldots, \xi_{i_n})$ denotes the polynomial chaos basis function of order n in terms of the random vector $\boldsymbol{\xi} = (\xi_{i_1}, \ldots, \xi_{i_n})$. The first basis function, Φ_0, has a constant value of 1. According to the theorem of Cameron and Martin [19], such expansions converge under the L_2 norm. For notational convenience, (14) is often rewritten as

$$X(\omega) = \sum_{j=0}^{\infty} \hat{a}_j \Psi_j(\boldsymbol{\xi}), \tag{15}$$

where there is a one-to-one correspondence between the functions $\Phi_n(\xi_{i_1}, \ldots, \xi_{i_n})$ and $\Psi_j(\boldsymbol{\xi})$. The $\{\Psi_j\}$ satisfy the orthogonality condition:

$$\mathbb{E}[\Psi_i \Psi_j] = \mathbb{E}[\Psi_i^2] \delta_{ij}. \tag{16}$$

According to relation (16), $\{\Psi_j\}$ is determined by the PDF of $\boldsymbol{\xi}$. The correspondence between classical PDFs and polynomials can be found in [5]. We note that the gPC basis can also be constructed numerically such that the above properties hold with the PDF of $\boldsymbol{\xi}$ as the weight function of orthogonal polynomials. Information on construction of such bases for arbitrary PDFs can be found in [20].

3.2. Model problem and assumptions

We consider the model problem

$$\mathscr{L}(\boldsymbol{x}, \omega; \boldsymbol{u}) = \boldsymbol{f}(\boldsymbol{x}, \omega), \tag{17}$$

where $\boldsymbol{x} \in \mathscr{D}$, $\omega \in \Omega$ and we seek a solution $\boldsymbol{u}(\boldsymbol{x}, \omega)$ which holds P-a.e. in Ω. The random inputs may come from the operator $\mathscr{L}$, right-hand side $\boldsymbol{f}$, and even the domain $\mathscr{D}$ (in the case of geometrically nonlinear elasticity, $\mathscr{D}$ is not a random input but nonetheless indirectly acquires a random dependence due to the nonlinearity in the problem). In order to solve problems such as (17) using the techniques discussed in this paper, an assumption of *finite dimensional noise* must be made for each random input $R(\omega)$:

$$R(\omega) = R(Y_1(\omega), Y_2(\omega), \ldots, Y_{d_r}(\omega)), \tag{18}$$

where the $\{Y_n\}_{n=1}^{d_r}$ are a finite set of real-valued random variables with mean zero and unit variance. Note that any stationary random process may be decomposed with a Karhunen–Loève expansion [21], whose truncated form satisfies the above assumptions (see Section 4 for more details). The case of non-independent or non-identically distributed $\{Y_i\}$ has been addressed in other papers such as [22], and can also be accommodated by the techniques in this paper. However, here we assume they are i.i.d. for simplicity in notation. The number of random variables will be denoted d_r, or the 'number of random dimensions', throughout the paper. We denote the range space of each variable $\Gamma_n \equiv Y_n(\Omega)$ and the product range space $\Gamma \equiv \prod_{n=1}^{d_r} \Gamma_n$ ($\boldsymbol{\Gamma} \equiv \boldsymbol{\Gamma}_1 \times \cdots \times \boldsymbol{\Gamma}_{\mathbf{d_r}}$). Since we have assumed the $\{Y_n\}_{n=1}^{d_r}$ are independent and continuous, they have a joint density function $\rho : \Gamma \to \mathbb{R}$, and

$$\rho(y) = \rho_1(y_1)\rho_2(y_2)\cdots\rho_{d_r}(y_{d_r}), \tag{19}$$

where the ρ_i are the corresponding density functions of the Y_i, $y_i \in \Gamma_i$ and $y = (y_1, y_2, \ldots, y_{d_r})$.

With this assumption, by the Doob–Dynkin lemma [23] we have that the solution $\boldsymbol{u}$ of (17) can also be described by a finite number of random variables:

$$\boldsymbol{u}(\boldsymbol{x}, \omega) = \boldsymbol{u}(\boldsymbol{x}, Y_1(\omega), Y_2(\omega), \ldots, Y_{d_r}(\omega)). \tag{20}$$

Let $\boldsymbol{Y} = (Y_1, Y_2, \ldots, Y_{d_r})$. Then, the goal of the numerical methods herein is to seek the solution $\boldsymbol{u}(\boldsymbol{x}, \boldsymbol{Y})$ to the problem:

$$\mathscr{L}(\boldsymbol{x}, \boldsymbol{Y}(\omega); \boldsymbol{u}) = f(\boldsymbol{x}, \boldsymbol{Y}(\omega)), \tag{21}$$

where $(\boldsymbol{x}, \omega) \in (\mathscr{D} \times \Omega)$.

3.3. Galerkin projection

Under these assumptions, all random quantities in the problem can be described by a finite number d_r of random variables as in (20). In addition, we assume that all the random processes involved reside in $L_2(\Omega, \mathscr{F}, P)$. The stochastic Galerkin method involves first expressing these random quantities as truncated gPC expansions in terms of the random vector $\boldsymbol{Y}$. For example, if the solution $\boldsymbol{u}$ is a spatial random process, we write

$$\boldsymbol{u}(\boldsymbol{x}, \omega) = \sum_{j=0}^{N_{\text{gpc}}} \hat{\boldsymbol{u}}_j(\boldsymbol{x}) \Psi_j(\boldsymbol{Y}), \tag{22}$$

where N_{gpc} is the number of terms in the truncated expansion, and is related to the number of random dimensions and the maximum polynomial order p by

$$N_{\text{gpc}}(p) = \frac{(d_r + p)!}{d_r! p!} - 1. \tag{23}$$

It is not necessary to use the same number of terms for every random quantity, but for simplicity we will assume this. We can then substitute these gPC expansions into Eq. (17) and perform a Galerkin projection $\mathbb{E}[\cdot, \Psi_i]$ onto each basis function. Through the orthogonality relation (16), we obtain a system of $N_{\text{gpc}} + 1$ deterministic equations for the unknown gPC coefficients $\hat{\boldsymbol{u}}_i$. Unless the problem is linear in random space, this system is coupled. Any standard numerical method can be used to solve this deterministic problem.

Once the coefficients of the expansion for $\boldsymbol{u}$ are found, the moments can be calculated easily due to the orthogonality condition. For example, the expected value of $\boldsymbol{u}$ is

$$\mathbb{E}[\boldsymbol{u}(\boldsymbol{x}, \boldsymbol{Y})] = \int \left(\sum_{i=0}^{N_{\text{gpc}}} \hat{\boldsymbol{u}}_i(\boldsymbol{x}) \Psi_i(\boldsymbol{Y}) \right) \rho(\boldsymbol{Y}) \, \mathrm{d}\boldsymbol{Y} = \hat{\boldsymbol{u}}_0 \tag{24}$$

and likewise the second moment is

$$\mathbb{E}[\boldsymbol{u}(\boldsymbol{x}, \boldsymbol{Y})^2] = \sum_{i=0}^{N_{\text{gpc}}} \hat{\boldsymbol{u}}_i^2 \mathbb{E}[\Psi_i^2]. \tag{25}$$

Many variations of the stochastic Galerkin method are found in the literature, including a multi-element formulation [24] and a multi-resolution formulation [25] based on multi-wavelet bases. However, as in deterministic Galerkin methods, the formulation of the deterministic coupled system can be quite difficult for complicated nonlinear problems. A numerical solver must be written for each specific system, and because of the coupling, these solvers are often computationally costly.

3.4. Collocation projection

The stochastic collocation method was first introduced by Tatang in [26] and has more recently been addressed in [11,27]. In this method, a set of collocation points $\{\boldsymbol{y}_i\}_{i=1}^{N_c}$ is defined on the space Γ. Collocation projections $\langle \cdot, \delta_{\boldsymbol{y}_i}(\boldsymbol{y}) \rangle$ are then performed on both sides of the model problem (21), obtaining:

$$\mathscr{L}(\boldsymbol{x}, \boldsymbol{y}_i; \boldsymbol{u}) = f(\boldsymbol{x}, \boldsymbol{y}_i), \quad i = 1, \ldots, N_c. \tag{26}$$

The resulting set of deterministic equations is always uncoupled and each solution $\boldsymbol{u}(\boldsymbol{x}, \boldsymbol{y}_i)$ may be found using a suitable numerical solver. The solution $\boldsymbol{u}$ as a function of $\boldsymbol{y}$ can then be approximated by interpolation on the $\{\boldsymbol{y}_i\}$. Solution moments can be found through numerical cubature. If the cubature weight function is chosen to coincide with the joint density ρ, then the expected value of $\boldsymbol{u}$ is simply

$$\mathbb{E}[\boldsymbol{u}(\boldsymbol{x}, t)] = \sum_{i=1}^{N_c} \boldsymbol{u}(\boldsymbol{x}, t, \boldsymbol{y}_i) w_c(\boldsymbol{y}_i), \tag{27}$$

where the w_c are the summation weights associated with the cubature rule. If they do not coincide, $\rho(\boldsymbol{y}_i)$ can be incorporated into the right-hand side of (27). Higher moments are calculated similarly.

While there are many options for obtaining a set of collocation points, in this paper we have chosen to use both full tensor product grids based of Chebyshev–Gauss–Lobatto points and sparse grids from the algorithm of Smolyak [28]. This approach was pioneered in [27] and also used in [11]. It has been extensively investigated in [29] for high-dimensional integration over cubes.

4. Representing random inputs: the Karhunen–Loève expansion

Consider a problem input, for example, the magnitude of normal fluid tractions, that we want to characterize as a spatially varying random process $T(\boldsymbol{x}, \omega)$, where $\omega \in \Omega$ and $\boldsymbol{x} \in \mathscr{D}$. The covariance kernel of this process, $R_{TT}(\boldsymbol{x}, \boldsymbol{y})$, relates the random field between two points in space as a function of the distance between them

$$R_{TT}(\boldsymbol{x}, \boldsymbol{y}) = \mathbb{E}[(T(\boldsymbol{x}) - \mathbb{E}[T(\boldsymbol{x})])(T(\boldsymbol{y}) - \mathbb{E}[T(\boldsymbol{y})])]. \tag{28}$$

The covariance kernel $R_{TT}(\boldsymbol{x}, \boldsymbol{y})$ is defined for all $\boldsymbol{x}$ and $\boldsymbol{y}$ in $\mathscr{D}$, the domain of our interest (for example, the surface on which pressure is uncertain, or the volume in which material properties are uncertain). By construction, the covariance kernel is real, symmetric, and positive-definite; thus it has an orthogonal set of eigenfunctions which forms a complete basis [7,21].

The Karhunen–Loève expansion is a representation of a random process in terms of a denumerable set of orthogonal random variables. For details regarding the error-minimizing property of this expansion, consult [7]. To find the correct expansion, we first find the eigenfunctions g_i and

eigen-values λ_i of the covariance function by solving the integral equation

$$\int_{\mathscr{D}} R_{TT}(\boldsymbol{x},\boldsymbol{y})g_i(\boldsymbol{x})\,\mathrm{d}\boldsymbol{x} = \lambda_i g_i(\boldsymbol{y}). \tag{29}$$

This integral may be solved explicitly in simple cases, such as a one-dimensional process with an exponential covariance kernel. However, in multi-dimensions with other covariance kernels (29) is solved numerically. A set of spatial covariance kernels, more appropriate for elliptic problems was formulated in [30]. Herein, we solve (29) numerically on a finite set of points.

Equipped with $g_i(\boldsymbol{x})$ and λ_i, we can write the following Karhunen–Loève expansion of T:

$$T(\boldsymbol{x},\omega) = \mathbb{E}[T(\boldsymbol{x})] + \sum_{i=1}^{\infty}\sqrt{\lambda_i}g_i(\boldsymbol{x})\xi_i(\omega), \tag{30}$$

where the ξ_i are a set of uncorrelated random variables with *zero mean* and *variance one* determined by

$$\xi_i(\omega) = \int_{\mathscr{D}} T(\boldsymbol{x};\omega)g_i(\boldsymbol{x})\,\mathrm{d}\boldsymbol{x}. \tag{31}$$

For example, if $T(\boldsymbol{x},\omega)$ is a Gaussian random process, then the ξ_i form a Gaussian vector. If $T(\boldsymbol{x},\omega)$ is a general second-order random process (not necessarily Gaussian), the joint probability density function of the $\{\xi\}_{i=1}^{\infty}$ is difficult to obtain. However, it is possible to estimate the marginal probability density functions using Eq. (31) and a density estimation technique. In this manner, one can approximate the PDF of the random variables in a finite-term K–L expansion; this has been addressed in [31]. Thus, the Karhunen–Loève decomposition separates the spatially varying components of the process from the random components. In practice, we take a truncated finite-term K–L expansion to represent our processes. To determine the number of terms to keep, we study the decay of the eigen-values λ_i, and truncate the series after their values decrease below 0.1% of the first eigenvalue.

Note that an expansion such as (30) can easily be written in the form of a gPC expansion, where a truncated K–L expansion with d_r terms fits into the zero and first-order terms of a d_r-dimensional gPC expansion. Thus, if the system of equations to be solved is decoupled, such as in the case of linear elasticity with stochastic loading, it is unnecessary to perform the computation with a polynomial order p any higher than 1 since the coefficients of higher order terms will always be zero.

5. Methodology for elasticity systems

In this section we formulate the methods described above in Sections 3.3 and 3.4 for the elasticity problems addressed in this paper. The first three sections present the gPC method for linear elasticity with stochastic material properties and traction boundary conditions. We present an algorithm for the stochastic material properties problem, which is nonlinear in random space and circumvents rewriting the original deterministic solver. The fourth and fifth sections consider the much simpler collocation formulation for linear and nonlinear elasticity with stochastic material properties and loading.

5.1. Case I: gPC formulation for linear elasticity system with E, ν deterministic, f random

We first formulate the stochastic Galerkin scheme for solving the linear elasticity with stochastic *loading*, which results in additive uncertainty. As we shall see, this is the simplest case of parametric uncertainty since the equations are linear in random space. We label this case of additive uncertainty for linear elasticity as Case I. In the numerical examples in Section 7 later, we will adopt the same labeling convention.

First, we expand the stochastic loading $\boldsymbol{f}$ and the solution $\boldsymbol{u}$ into their gPC representations. $\forall\omega\in\Omega$,

$$\begin{aligned}\boldsymbol{u}(\boldsymbol{x},\omega) &= \sum_{i=0}^{N_{\mathrm{gpc}}}\hat{\boldsymbol{u}}_i(\boldsymbol{x})\Psi_i(\boldsymbol{\xi}(\omega)),\\ \boldsymbol{f}(\boldsymbol{x},\omega) &= \sum_{i=0}^{N_{\mathrm{gpc}}}\hat{\boldsymbol{f}}_i(\boldsymbol{x})\Psi_i(\boldsymbol{\xi}(\omega)).\end{aligned} \tag{32}$$

As noted in Section 4, if the loading input is represented by a Karhunen–Loève expansion with d_r+1 terms, this can easily be written as an equivalent gPC expansion as in Eq. (32) with the coefficients $\hat{\boldsymbol{f}}_i = 0$ for all $i = d_r+1$, $d_r+2,\ldots,N_{\mathrm{gpc}}$. In this and future sections, we consider the general form of the gPC expansion for the random input. Next we substitute the above into Eq. (5) (expressed in terms of E and ν) and take the Galerkin projection $\langle\cdot,\Psi_k\rangle$:

$$\begin{aligned}&-\frac{E(\boldsymbol{x})}{2(1+\nu(\boldsymbol{x}))}\nabla^2\hat{\boldsymbol{u}}_k(\boldsymbol{x}) - \frac{E(\boldsymbol{x})}{2(1+\nu(\boldsymbol{x}))(1-2\nu(\boldsymbol{x}))}\nabla(\nabla\cdot\hat{\boldsymbol{u}}_k(\boldsymbol{x}))\\ &= \hat{\boldsymbol{f}}_k(\boldsymbol{x})\end{aligned} \tag{33}$$

for $k = 0,1,\ldots,N_{\mathrm{gpc}}$. In this case the equations are decoupled. If the random input has only first-order terms in its expansion, as in the case of a truncated K–L expansion, then there is no gain in using a gPC expansion with polynomial order greater than one. In that case we only need to solve $(N_{\mathrm{gpc}}+1) = n+1$ deterministic equations using a standard FEM solver, where n is the index of the last term in the K–L expansion.

5.2. Case II: gPC formulation for linear elasticity system with E, ν random, f deterministic

In the case of stochastic material properties, we obtain multiplicative uncertainty and therefore a nonlinearity in random space. We now formulate the gPC scheme for stochastic material properties and label this Case II.

5.2.1. Formulating the coupled system

First, we expand E, v and the solution $\boldsymbol{u}$ into their gPC representations. $\forall \omega \in \Omega$,

$$\begin{aligned} \boldsymbol{u}(\boldsymbol{x},\omega) &= \sum_{i=0}^{N_{\text{gpc}}} \hat{\boldsymbol{u}}_i(\boldsymbol{x})\Psi_i(\boldsymbol{\xi}(\omega)), \\ E(\boldsymbol{x},\omega) &= \sum_{i=0}^{N_{\text{gpc}}} \widehat{E}_i(\boldsymbol{x})\Psi_i(\boldsymbol{\xi}(\omega)), \\ v(\boldsymbol{x};\omega) &= \sum_{i=0}^{N_{\text{gpc}}} \hat{v}_i(\boldsymbol{x})\Psi_i(\boldsymbol{\xi}(\omega)). \end{aligned} \tag{34}$$

Next we substitute these into Eq. (5):

$$\begin{aligned} &-\sum_{i=0}^{N_{\text{gpc}}}\sum_{j=0}^{N_{\text{gpc}}} \frac{\widehat{E}_i(\boldsymbol{x})}{2(1+\hat{v}_i(\boldsymbol{x}))}\nabla^2\hat{\boldsymbol{u}}_j(\boldsymbol{x})\Psi_i\Psi_j \\ &\quad -\sum_{i=0}^{N_{\text{gpc}}}\sum_{j=0}^{N_{\text{gpc}}} \frac{\widehat{E}_i(\boldsymbol{x})}{2(1+\hat{v}_i(\boldsymbol{x}))(1-2\hat{v}_i(\boldsymbol{x}))}\nabla(\nabla\cdot\hat{\boldsymbol{u}}_j(\boldsymbol{x}))\Psi_i\Psi_j \\ &\quad = \boldsymbol{f}(\boldsymbol{x}), \end{aligned} \tag{35}$$

and take the Galerkin projection $\langle\cdot,\Psi_k\rangle$:

$$\begin{aligned} &-\sum_{i=0}^{N_{\text{gpc}}}\sum_{j=0}^{N_{\text{gpc}}} \langle\Psi_i\Psi_j\Psi_k\rangle\frac{\widehat{E}_i(\boldsymbol{x})}{2(1+\hat{v}_i(\boldsymbol{x}))}\nabla^2\hat{\boldsymbol{u}}_j(\boldsymbol{x}) \\ &\quad -\sum_{i=0}^{N_{\text{gpc}}}\sum_{j=0}^{N_{\text{gpc}}} \langle\Psi_i\Psi_j\Psi_k\rangle\frac{\widehat{E}_i(\boldsymbol{x})}{2(1+\hat{v}_i(\boldsymbol{x}))(1-2\hat{v}_i(\boldsymbol{x}))}\nabla(\nabla\cdot\hat{\boldsymbol{u}}_j(\boldsymbol{x})) \\ &\quad = \hat{\boldsymbol{f}}_k(\boldsymbol{x}) \end{aligned} \tag{36}$$

for $k = 0,1,\ldots,N_{\text{gpc}}$ where $\hat{\boldsymbol{f}}_k(\boldsymbol{x}) = \boldsymbol{f}(\boldsymbol{x})$ if $k = 0$, and zero otherwise.

5.2.2. Solving the coupled system

As mentioned previously, we assume that the body forces are deterministic, i.e.

$$\langle \boldsymbol{f}\Psi_k\rangle \overset{\text{def}}{=} \boldsymbol{f}_k = \begin{cases} \boldsymbol{f}, & k = 0, \\ 0, & k \neq 0. \end{cases}$$

Likewise, if any tractions $\boldsymbol{T}$ are prescribed on $\partial\Gamma_T$, we assume they are deterministic, so that

$$\langle \boldsymbol{T}\Psi_k\rangle \overset{\text{def}}{=} \boldsymbol{T}_k = \begin{cases} \boldsymbol{T}, & k = 0, \\ 0, & k \neq 0. \end{cases}$$

We define

$$b_{jk} = \sum_{i=0}^{N_{\text{gpc}}}\langle\Psi_j\Psi_i\Psi_k\rangle\frac{\widehat{E}_i(\boldsymbol{x})}{2(1+\hat{v}_i(\boldsymbol{x}))}, \tag{37}$$

$$d_{jk} = \sum_{i=0}^{N_{\text{gpc}}}\langle\Psi_j\Psi_i\Psi_k\rangle\frac{\widehat{E}_i(\boldsymbol{x})}{2(1+\hat{v}_i(\boldsymbol{x}))(1-2\hat{v}_i(\boldsymbol{x}))} \tag{38}$$

and the Navier–Lamé (N–L) elasticity operator associated with the material properties above by

$$\mathscr{L}_{jk}(\boldsymbol{x}) \overset{\text{def}}{=} b_{jk}(\boldsymbol{x})\nabla^2 + d_{jk}(\boldsymbol{x})\nabla(\nabla\cdot), \tag{39}$$

where any two N–L operators having different subscripts differ simply by the material properties.

Then, (36) can also be written as

$$\sum_{j=0}^{N_{\text{gpc}}}\mathscr{L}_{jk}(\boldsymbol{x})(\boldsymbol{u}_j(\boldsymbol{x})) = -\boldsymbol{f}_k(\boldsymbol{x}), \quad k = 0,1,2\ldots,N_{\text{gpc}}, \tag{40}$$

where this system can be seen as $(j+1)\times(k+1)$ coupled N–L systems.

Multiplying each of the $(N_{\text{gpc}}+1)$ equations in (40) by a test function $\boldsymbol{v}_k$, and in view of (9), we obtain the weak formulation corresponding to (40):

Find $\boldsymbol{u}_j \in [\overset{\circ}{\mathscr{E}}(\mathscr{D})]^{N_{\text{gpc}}+1}$ so that

$$\begin{aligned} &\sum_{j=0}^{P}\mathscr{B}_{jk}(\boldsymbol{u}_j,\boldsymbol{v}_k) = \mathscr{F}_k^{\text{BF}}(\boldsymbol{v}_k) + \mathscr{F}_k^{\text{T}}(\boldsymbol{v}_k) \quad \forall \boldsymbol{v}_k \in [\overset{\circ}{\mathscr{E}}(\mathscr{D})]^{N_{\text{gpc}}+1}, \\ &\quad k = 0,1,\ldots,N_{\text{gpc}}, \end{aligned} \tag{41}$$

where to simplify notation we have dropped the $(\boldsymbol{x})$ denoting spatially varying functions and operators, and $\mathscr{B}_{jk}$ is the elasticity bilinear form (9) with material properties according to $b_{jk}(\boldsymbol{x})$ and $d_{jk}(\boldsymbol{x})$ in (37), (38). This equation (41) is assumed to be well-posed, although not proven herein. Indications on the well-posedness are evident in the numerical examples in later sections, where we solve (41) iteratively with very fast convergence (within 5–6 iterations). The reader is referred to [10] for more discussion on the well-posedness of gPC formulations of stochastic elliptic problems.

Discretizing the weak formulation by the finite element method and taking $\boldsymbol{u}_j = \boldsymbol{a}_j[N]$ (where $[N]$ is the shape function matrix) a matrix representation is obtained, which can be written as

$$\sum_{j=0}^{N_{\text{gpc}}}[K_{jk}]\boldsymbol{a}_j = \boldsymbol{F}_k^{\text{BF}} + \boldsymbol{F}_k^{\text{T}} \overset{\text{def}}{=} \boldsymbol{F}_k, \quad k = 0,1,\ldots,N_{\text{gpc}}. \tag{42}$$

Here $[K_{jk}]$ is the stiffness matrix associated with the entire domain $\mathscr{D}$ with spatially varying material properties $b_{jk}(\boldsymbol{x})$ and $d_{jk}(\boldsymbol{x})$, and the $\boldsymbol{F}_k$ are the load vectors. A high-dimensional coupled linear system of algebraic equations is obtained. For example, if the dimension of the stiffness matrix (number of degrees of freedom) is DOF, then the overall dimension of the coupled system is $(N_{\text{gpc}}+1)\times DOF$. Instead of inverting directly such a large system, we use an iterative scheme, such that it is first transformed into a "decoupled" form. We leave the kth term in the sum to remain in the LHS of the equation, and move all other terms to the RHS to obtain:

$$[K_{kk}]\boldsymbol{a}_k = \boldsymbol{F}_k - \sum_{j=0,\ j\neq k}^{N_{\text{gpc}}}[K_{jk}]\boldsymbol{a}_j, \quad k = 0,1,\ldots,N_{\text{gpc}}. \tag{43}$$

The decoupling is achieved by choosing in the RHS, instead of the unknown solution vectors $\boldsymbol{a}_j$, the solution vectors in the previous iteration to compute a better

approximation; we obtain the following iterative scheme for the solution of the coupled system:

$$\boldsymbol{a}_k^{(n+1)} = [K_{kk}]^{-1}\boldsymbol{F}_k - \sum_{j=0,\ j\neq k}^{N_{\mathrm{gpc}}} [K_{kk}]^{-1}[K_{jk}]\boldsymbol{a}_j^{(n)}, \quad k = 0,1,\ldots,N_{\mathrm{gpc}}. \tag{44}$$

For deterministic body forces and tractions, (44) reduces to

$$\boldsymbol{a}_0^{(n+1)} = [K_{00}]^{-1}\boldsymbol{F}_0 - \sum_{j=1}^{N_{\mathrm{gpc}}}[K_{00}]^{-1}[K_{j0}]\boldsymbol{a}_j^{(n)}, \tag{45}$$

$$\boldsymbol{a}_k^{(n+1)} = -\sum_{j=0,\ j\neq k}^{N_{\mathrm{gpc}}} [K_{kk}]^{-1}[K_{jk}]\boldsymbol{a}_j^{(n)}, \quad k = 1,\ldots,N_{\mathrm{gpc}} \tag{46}$$

and the iterative procedure uses the initial guess

$$\boldsymbol{a}_0^{(0)} = [K_{00}]^{-1}\boldsymbol{F}_0, \tag{47}$$

$$\boldsymbol{a}_k^{(0)} = \boldsymbol{0}, \quad k = 1,\ldots,N_{\mathrm{gpc}}. \tag{48}$$

To accelerate the convergence rate of (45), (46), the Gauss–Seidel algorithm is employed (we use in the $(n+1)$th iteration of the kth coefficient the n previously computed values of the $k-1$ coefficients). In other words,

$$\boldsymbol{a}_0^{(n+1)} = [K_{00}]^{-1}\boldsymbol{F}_0 - \sum_{j=1}^{N_{\mathrm{gpc}}}[K_{00}]^{-1}[K_{j0}]\boldsymbol{a}_j^{(n)}, \tag{49}$$

$$\boldsymbol{a}_k^{(n+1)} = -\sum_{j=0}^{k-1}[K_{kk}]^{-1}[K_{jk}]\boldsymbol{a}_j^{(n+1)} - \sum_{j=k+1}^{N_{\mathrm{gpc}}}[K_{kk}]^{-1}[K_{jk}]\boldsymbol{a}_j^{(n)}, \quad k = 1,\ldots,N_{\mathrm{gpc}}. \tag{50}$$

5.2.3. An efficient algorithm for the case of stochastic Young's modulus

For the special case in which only E, the Young's modulus, is random:

$$b_{jk}(\boldsymbol{x}) = \frac{1}{2(1+\nu)}\sum_{i=0}^{N_{\mathrm{gpc}}}\langle\Psi_j\Psi_i\Psi_k\rangle E_i(\boldsymbol{x}), \tag{51}$$

$$d_{jk}(\boldsymbol{x}) = \frac{1}{2(1+\nu)(1-2\nu)}\sum_{i=0}^{N_{\mathrm{gpc}}}\langle\Psi_j\Psi_i\Psi_k\rangle E_i(\boldsymbol{x}). \tag{52}$$

Now, let

$$E_{jk}(\boldsymbol{x}) \overset{\mathrm{def}}{=} \sum_{i=0}^{N_{\mathrm{gpc}}}\langle\Psi_j\Psi_i\Psi_k\rangle E_i(\boldsymbol{x}). \tag{53}$$

In view of the large dimension of the system obtained, the computational time required to solve (49), (50) may be very high, especially for high P_{FEM} levels where the stiffness matrices are large and one needs to perform multiple matrix multiplications.

For *linear* elasticity problems it is possible to shorten the computational time considerably, by the following procedure. Since the stiffness matrices $[K_{jk}]$ are all for same domain $\mathscr{D}$ and differ only by the Young's modulus (E_{jk}), then only one stiffness matrix needs to be computed. For example, compute $[K_{00}]$ so that any $[K_{jk}]$ can be obtained by a simple multiplication

$$[K_{jk}] = \frac{E_{jk}}{E_{00}}[K_{00}]. \tag{54}$$

It follows immediately from (54) that:

$$[K_{jk}^{-1}] = \frac{E_{00}}{E_{jk}}[K_{00}^{-1}]. \tag{55}$$

Substituting (54), (55) into (49), (50), one obtains the following system:

$$\boldsymbol{a}_0^{(n+1)} = [K_{00}]^{-1}\boldsymbol{F}_0 - \sum_{j=1}^{N_{\mathrm{gpc}}}\frac{E_{j0}}{E_{00}}\boldsymbol{a}_j^{(n)}, \tag{56}$$

$$\boldsymbol{a}_k^{(n+1)} = -\sum_{j=0}^{k-1}\frac{E_{jk}}{E_{kk}}\boldsymbol{a}_j^{(n+1)} - \sum_{j=k+1}^{N_{\mathrm{gpc}}}\frac{E_{jk}}{E_{kk}}\boldsymbol{a}_j^{(n)}, \quad k = 1,\ldots,N_{\mathrm{gpc}}. \tag{57}$$

Thus, it is clear that in the case of linear elasticity, one needs to generate the stiffness matrix only once, and then use the Gauss–Seidel algorithm with a fraction of the operations needed as compared to the previous section.

The algorithm for a standard FE code is

- Compute the matrix E_{jk}.
- Generate the FE model for the domain of interest, including the deterministic boundary conditions.
- Read from a file the *upper triangular E matrix* (as $E_{jk} = E_{kj}$) for $i,j = 0,\ldots,N_{\mathrm{gpc}}$, and start a loop on the FE solver.
- Update the material property E (being a parameter) in the FE solver.
- Compute the global constrained stiffness matrix and load vector and output them into a file.
- Read the upper triangular part of stiffness matrix and load vector and store them into arrays.
- Perform the iterative procedure according to (49), (50).
- Check convergence by the relative difference of two consecutive solutions of $\boldsymbol{a}_j$.
- Read the set of points at which output is required.
- Start a loop where $j = 0,1,\ldots,,N_{\mathrm{gpc}}$ to upload the solution vector $\boldsymbol{a}_j$ to the FE solver, and using the solution vector compute the displacements at the points of interest.

Note that in the case where both E and ν are random, a similar algorithm can be used. However, in this case the stiffness matrix cannot be obtained by a single multiplication anymore. In the numerical examples following, we take only the Young's modulus to be stochastic. However, we will continue to address the more general case through the formulation sections.

5.3. Combined additive and multiplicative uncertainty – E, ν and $\boldsymbol{f}$ random

Here we formulate the problem for the linear elasticity case when both material properties and loadings are ran-

dom. Although we do not show a numerical example of this case, the methods presented in this work are easily generalized to accommodate additive and multiplicative uncertainty. If we follow the same steps as above, we obtain the coupled set of deterministic equations:

$$-\sum_{i=0}^{N_{\text{gpc}}}\sum_{j=0}^{N_{\text{gpc}}}\frac{\langle\Psi_i\Psi_j\Psi_k\rangle}{\langle\Psi_k^2\rangle}\frac{\widehat{E}_i(\boldsymbol{x})}{2(1+\hat{\nu}_i(\boldsymbol{x}))}\nabla^2\hat{\boldsymbol{u}}_j(\boldsymbol{x}) - \sum_{i=0}^{N_{\text{gpc}}}\sum_{j=0}^{N_{\text{gpc}}}\frac{\langle\Psi_i\Psi_j\Psi_k\rangle}{\langle\Psi_k^2\rangle}\frac{\widehat{E}_i(\boldsymbol{x})}{2(1+\hat{\nu}_i(\boldsymbol{x}))(1-2\hat{\nu}_i(\boldsymbol{x}))}\nabla(\nabla\cdot\hat{\boldsymbol{u}}_j(\boldsymbol{x})) = \hat{\boldsymbol{f}}_k(\boldsymbol{x}) \tag{58}$$

for $k = 0, 1, \ldots, N_{\text{gpc}}$.

5.3.1. Solving the coupled system

Here the forcing on the RHS of (58) is random so we will have non-zero $\boldsymbol{f}_k$ for $k \neq 0$. Define

$$b_{jk} \overset{\text{def}}{=} \sum_{i=0}^{N_{\text{gpc}}}\frac{\langle\Psi_j\Psi_i\Psi_k\rangle}{\langle\Psi_k^2\rangle}\frac{\widehat{E}_i(\boldsymbol{x})}{2(1+\hat{\nu}_i(\boldsymbol{x}))},$$

$$d_{jk} \overset{\text{def}}{=} \sum_{i=0}^{N_{\text{gpc}}}\frac{\langle\Psi_j\Psi_i\Psi_k\rangle}{\langle\Psi_k^2\rangle}\frac{\widehat{E}_i(\boldsymbol{x})}{2(1+\hat{\nu}_i(\boldsymbol{x}))(1-2\hat{\nu}_i(\boldsymbol{x}))}.$$

The resulting FEM formulation is identical to (44), except for the factor of $\langle\Psi_k^2\rangle$ in the denominator. The initial guess for the iterative algorithm is

$$\boldsymbol{a}_k^{(0)} = [K_{kk}]^{-1}\boldsymbol{F}_k, \quad k = 0, 1, \ldots, N_{\text{gpc}} \tag{59}$$

and the iterative scheme to be solved becomes

$$\boldsymbol{a}_k^{(n+1)} = [K_{kk}]^{-1}\boldsymbol{F}_k - \sum_{j=0}^{k-1}[K_{kk}]^{-1}[K_{jk}]\boldsymbol{a}_j^{(n+1)} - \sum_{j=k+1}^{N_{\text{gpc}}}[K_{kk}]^{-1}[K_{jk}]\boldsymbol{a}_j^{(n)}, \quad k = 1, \ldots, N_{\text{gpc}}. \tag{60}$$

Numerical examples using the gPC method for Cases I and II are provided in Section 7, after we first introduce the stochastic collocation formulation for linear and nonlinear elasticity problems.

5.4. Case III: Collocation scheme for linear/nonlinear elasticity systems with E, ν random, f deterministic

As seen in the previous sections the gPC method for problems with nonlinearities in random space (such as those with stochastic Young's modulus) require the solving of a coupled problem using an iterative solver. To add another level of complexity and solve the geometrically nonlinear elasticity formulation using the gPC method would require an extremely complicated formulation for the scheme as well as a time-consuming computation. Thus, in this section we apply the stochastic collocation method to linear and geometrically nonlinear elasticity problems with random Young's modulus. Suppose we have a stochastic E, characterized by a finite number of random variables, $\{Y_n\}_{n=1}^{d_r}$, and a set of cubature points $\{\boldsymbol{y}_i\}_{i=1}^{N_c}$ in the corresponding range space of the random variables, Γ.

In the case of linear elasticity, we would like to solve the following problem for $\boldsymbol{u}(\boldsymbol{x}, \boldsymbol{y}_i)$:

$$-\frac{E(\boldsymbol{x},\boldsymbol{y}_i)}{2(1+\nu(\boldsymbol{x},\boldsymbol{y}_i))}\nabla^2\boldsymbol{u}(\boldsymbol{x},\boldsymbol{y}_i) - \frac{E(\boldsymbol{x},\boldsymbol{y}_i)}{2(1+\nu(\boldsymbol{x},\boldsymbol{y}_i))(1-2\nu(\boldsymbol{x},\boldsymbol{y}_i))}\nabla(\nabla\cdot\boldsymbol{u}(\boldsymbol{x},\boldsymbol{y}_i)) = \boldsymbol{f}(\boldsymbol{x}) \quad \text{in } \mathscr{D} \tag{61}$$

for each $i \in \{1, 2, \ldots, N_c\}$ with the usual boundary conditions given in (7).

Note that here E and ν have both a spatial and random dependence. In the numerical examples following, we assume these properties to be constant throughout the material for each random realization (see Section 2 for more discussion).

Similarly, for the case of nonlinear elasticity we solve (8) and (10) for each C^i_{lmno} associated with the Young's modulus value specified by each collocation point. After solving for the solution $\boldsymbol{u}(\boldsymbol{x}, \boldsymbol{y}_i)$ at each collocation point, we may then interpolate over random space or take statistical moments of the solution through relations such as (27).

5.5. Case IV: Collocation scheme for linear/nonlinear elasticity systems with E, ν deterministic, f random

In this section we formulate the stochastic collocation method for linear and geometrically nonlinear elasticity problems with random traction loadings. Supposed we would like the mean loading $(C_p)_{\text{exp}}(\theta)$ to be as defined in (13). Then define two-dimensional random loadings to be $(C_p)_{\text{exp}}(\theta)(1+\alpha\xi_1)+\beta\xi_2$ where ξ_1 and ξ_2 are independent random variables uniformly distributed on $[-1, 1]$, and α and β are constants specifying the amplitude of the noise. In this example we have a low number of random dimensions ($d_r = 2$). As will be seen later, this is chosen in order to investigate the effect of the 'sparseness' of the collocation grid in the numerical examples. In other words, we consider the cost associated with using fewer collocation points in a Smolyak sparse grid versus a full tensor product collocation grid. However, this method is obviously valid for more general random inputs with more dimensions.

Suppose we have a full or sparse set of N_c cubature points for the two-dimensional random input specified above: $\{(q_i, p_i)\}_{i=1}^{N_c}$ in $[-1, 1]\times[-1, 1]$. In the case of linear elasticity, we solve (5)–(7) for u, with traction boundary conditions given by $(C_p)_{\text{exp}}(\theta)(1+\alpha q_i)+\beta p_i$ for each $i \in \{1, 2, \ldots, M\}$.

Similarly, for the case of nonlinear elasticity we solve (8) and (10) with follower-load traction boundary conditions (11) given by $(C_p)_{\text{exp}}(\theta)(1+\alpha q_i)+\beta p_i$ for each $i \in \{1, 2, \ldots, N_c\}$.

It is easy to see that if both the material properties and loading are random this method works in the same way.

6. Prescribing a random loading

In Case I we prescribe a stochastic process for the traction boundary conditions, using the K–L expansion to express it in terms of a gPC basis. We begin with the model of fluid flow past the circular cylinder with attached mass (see Fig. 2(right)). The mean flow pressure profile $T_{\exp}(\boldsymbol{x})$ is taken from experimental data [15]. We impose a stochastic perturbation characterized as a Gaussian random process with a covariance kernel of the form

$$R_{TT}(\boldsymbol{x},\boldsymbol{y}) = \mathrm{e}^{-\frac{\|\boldsymbol{x}-\boldsymbol{y}\|^2}{A}}, \tag{62}$$

where A is the correlation length of the process and $\boldsymbol{x},\boldsymbol{y} \in \mathscr{D}$. This process varies spatially on the outer surface of the object, corresponding to a situation in which the fluid velocity outside the cylinder undergoes random fluctuations.

In the present case, $A = 6$ and the standard deviation of the process, $\sigma = 1$. The mean tractions range from approximately -10^2 to $10^2\,\mathrm{N/m^2}$, so the standard deviation is approximately 1% of the loading at its maximum (see (13)). However, at angles around the cylinder where the loading is below its maximum, this noise level constitutes a much higher percentages of the mean loading. For the computation of Askey polynomials and the corresponding eigenvalues, the structure is meshed with twelve finite elements and 616 degrees of freedom (N), obtained by Gauss–Jacobi quadrature on the mapped standard element (see Fig. 3).

We numerically calculate the eigen-values λ_i and eigenfunctions $g_i(\boldsymbol{x}^n)$ of the covariance kernel at each mesh point, where the superscript represents the degree of freedom $n = 1,2,\ldots 616$. Fig. 4 shows the decay of the first 40 eigenvalues. We truncate the series after the term $i = 19$, such that $\lambda_{19}/\lambda_1 \leqslant 0.001$.

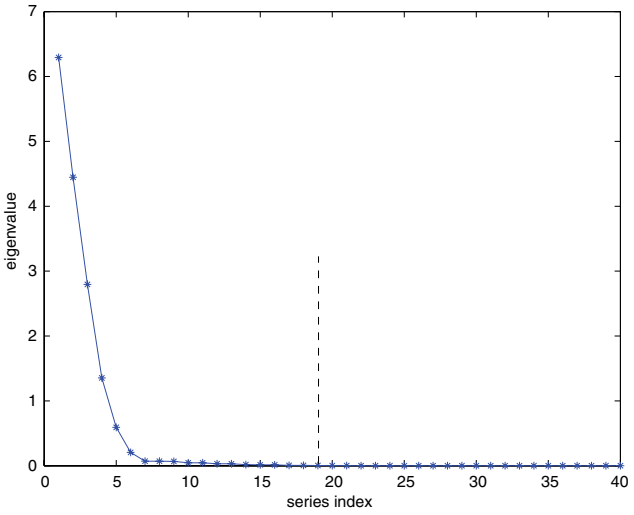

Fig. 4. Eigenvalue decay. The dashed line represents the term after which the series is truncated.

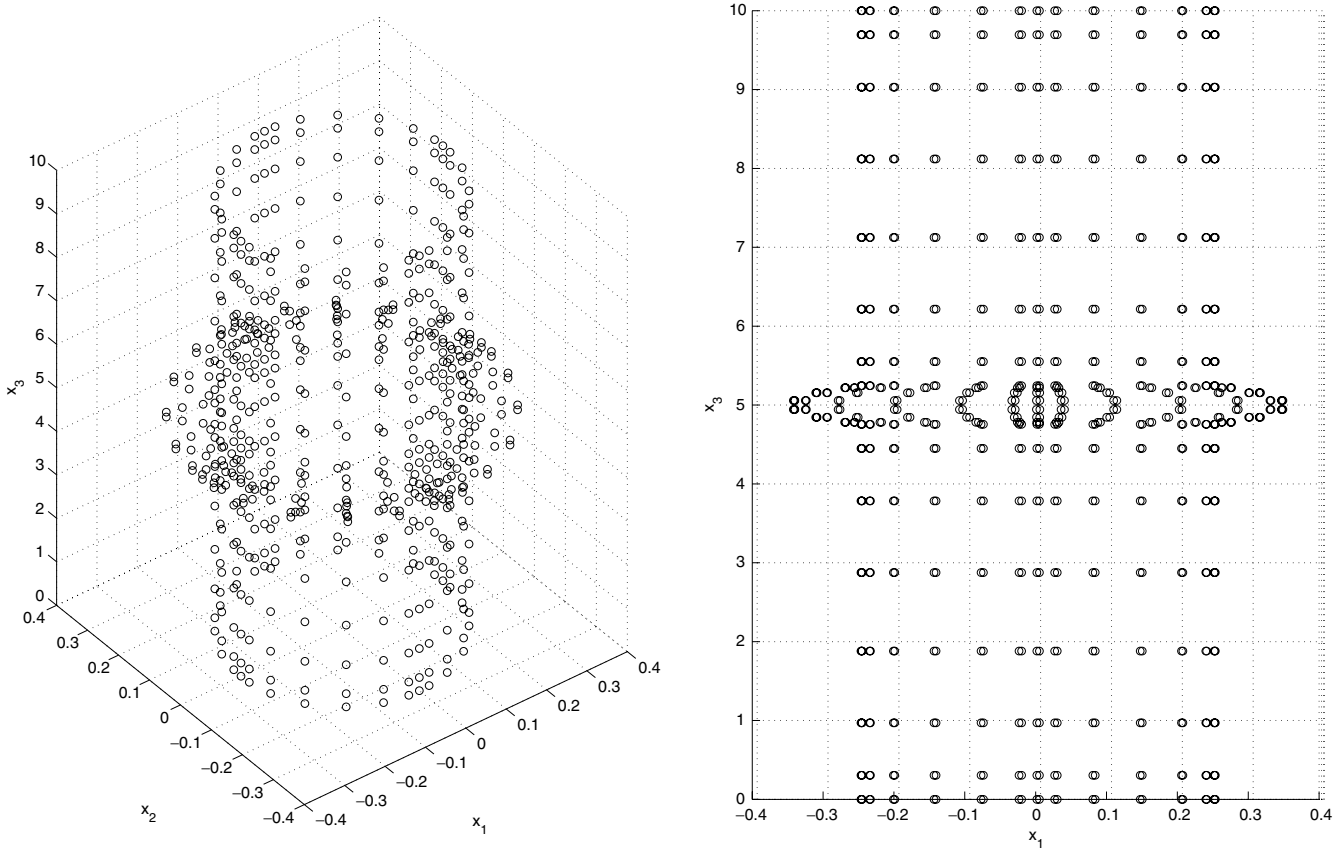

Fig. 3. Grid points at which the K–L representation is computed (isometric view and view from along the x_2 axis, looking towards the origin).

Now, our Karhunen–Loéve expansion is written as

$$T(\boldsymbol{x}^n;\omega) = T_{\exp}(\boldsymbol{x}^n) + \sigma \sum_{i=1}^{19} \sqrt{\lambda_i} g_i(\boldsymbol{x}^n)\xi_i(\omega), \tag{63}$$

where $n = 1,2,\ldots,N$ and the ξ_i are independent, identically distributed Gaussian random variables with mean zero and variance one.

7. Numerical examples

7.1. Case I

We consider the tube with attached mass, shown in Fig. 1A and B, with deterministic Young's modulus given by the mean value for 4140 steel ($E = 212.74$ GPa) [16]. For the stochastic loading we use the K–L eigenfunctions g_i computed in Section 6. Because we use a finite element solver as a "black box", we need to approximate each of the numerically computed functions g_k by a least mean square (LMS) approximation to be applied as traction boundary conditions. Thus, each g_k is approximated by

$$(\mathscr{P}g)_k = \sum_{i=0,j=0}^{p_\theta,p_z} a_{ij}^k h_i(\theta) z^j, \tag{64}$$

where

$$h_i(\theta) = \begin{cases} \cos(i\theta/2), & i = 0,2,4,6,\ldots, \\ \sin((i+1)/2), & i = 1,3,5,7,\ldots \end{cases} \tag{65}$$

such that a_{ij}^k are determined by minimizing $\sum_{i=1}^N [(\mathscr{P}g)_k(\boldsymbol{x}^i) - g_k(\boldsymbol{x}^i)]^2$, where N is the number of degrees of freedom in the domain.

7.1.1. P_{LMS} error

We investigate the error in approximating the Karhunen–Loève eigenfunctions using the least mean squares (LMS) method. Here we study the convergence in p_θ and p_z as the order of LMS approximation functions increases. These results reflect the LMS convergence for the linear elasticity case. We define and evaluate a pointwise relative error ϵ_k on the domain, where k represents the kth eigenfunction:

$$\epsilon_k = \frac{1}{N}\sqrt{\frac{\sum_{i=1}^N (g_k(\boldsymbol{x}^i) - \mathscr{P}g_k(\boldsymbol{x}^i))^2}{\sum_{i=1}^N g_k(\boldsymbol{x}^i)^2}}. \tag{66}$$

Fig. 6 shows this error for each of the $(N_{\text{gpc}} + 1) = 20$ loading functions, at 6 levels of P_{LMS}.

These results reflect the good LMS convergence for the approximation of the K–L loading functions, and in the sequel we use $p_\theta = 18$ and $p_z = 6$ in all subsequent analyses.

7.1.2. gPC analysis

As seen in (33), we need to solve $(N_{\text{gpc}} + 1)$ deterministic decoupled problems for the stochastic loading system. In this case, $N_{\text{gpc}} = 19$ since we have $d_r = 19$ eigenpairs in our truncated K–L expansion and $p = 1$ for the reasons detailed in Section 4. The zeroth mode corresponds to the deterministic problem with mean loading. For each of the $(N_{\text{gpc}} + 1)$ problems, we prescribe $(\mathscr{P}g)_k$ as the pressure on the outer surface of the cylinder. A few examples of the various $(\mathscr{P}g)_k$ for $p_\theta = 18$ and $p_z = 6$ are shown in Fig. 5. We solve each of these 20 problems separately, and then find the mean and variance of our stochastic solution using Eqs. (24) and (25).

We perform linear elastic analyses using a finite element spatial discretization of orders $P_{\text{FEM}} = 5,6,7$ on the coarse mesh (Fig. 1B) and $P_{\text{FEM}} = 7, 8$ on the mesh refined in the vicinity of the singular edges (Fig. 1A) to investigate the influence of the spatial discretization on the mean and variance of the displacements. Fig. 7 shows the mean and variance of the displacement in x_1 direction (i.e., u_1) on surface slices of the cylinder for the refined mesh with $P_{\text{FEM}} = 8$. The angle $\theta = 0$ represents the mean stagnation point of the flow. In Fig. 8 we plot the pointwise relative difference of the mean and variance of u_1 for $P_{\text{FEM}} = 5,6,7$ on the coarse mesh and $P_{\text{FEM}} = 7$ on the fine mesh as compared to $P_{\text{FEM}} = 8$ on the fine mesh. Here we define the error between two functions $u(\boldsymbol{x}^i)$ and $v(\boldsymbol{x}^i)$ where $\boldsymbol{x}^i$ are the points in the domain

$$\epsilon = \frac{1}{N}\sqrt{\frac{\sum_{i=1}^N (u(\boldsymbol{x}^i) - v(\boldsymbol{x}^i))^2}{\sum_{i=1}^N v(\boldsymbol{x}^i)^2}}. \tag{67}$$

This error definition is identical to the one used in (66) but we restate it here in more general notation, where the function v is taken to be the reference result. One may observe that a good convergence in spatial discretization is obtained, and the results on the fine mesh at $P_{\text{FEM}} = 8$ are considered to be converged.

7.1.3. Comparison with Monte-Carlo simulations

Monte-Carlo simulation performed *after* Karhunen–Loéve expansion is the process in which the random variables ξ_i in the K–L expansion are simulated instead of the actual random process. In other words, we draw one instance of each of the 19 random variables in the K–L expansion, construct the loading and solve the elasticity problem for each Monte-Carlo run. Since the uncertainty is linear in random space as well as physical space, solving this problem is equivalent to solving the elasticity system for each input separately and taking the linear combination of solutions. It is easy to see then that the gPC solution theoretically gives the solution to which Monte-Carlo *after* K–L converges. Thus, there is no need to perform Monte-Carlo simulations to verify the accuracy of the numerical results. Nevertheless, to obtain an estimate of the number of samples it would take to simulate the result, a post-processing MC simulation was run at $P_{\text{FEM}} = 8$ on the refined mesh. The solution was found to converge in variance to the gPC result at the same spatial discretization level after approximately 1000 iterations. We note that this simple

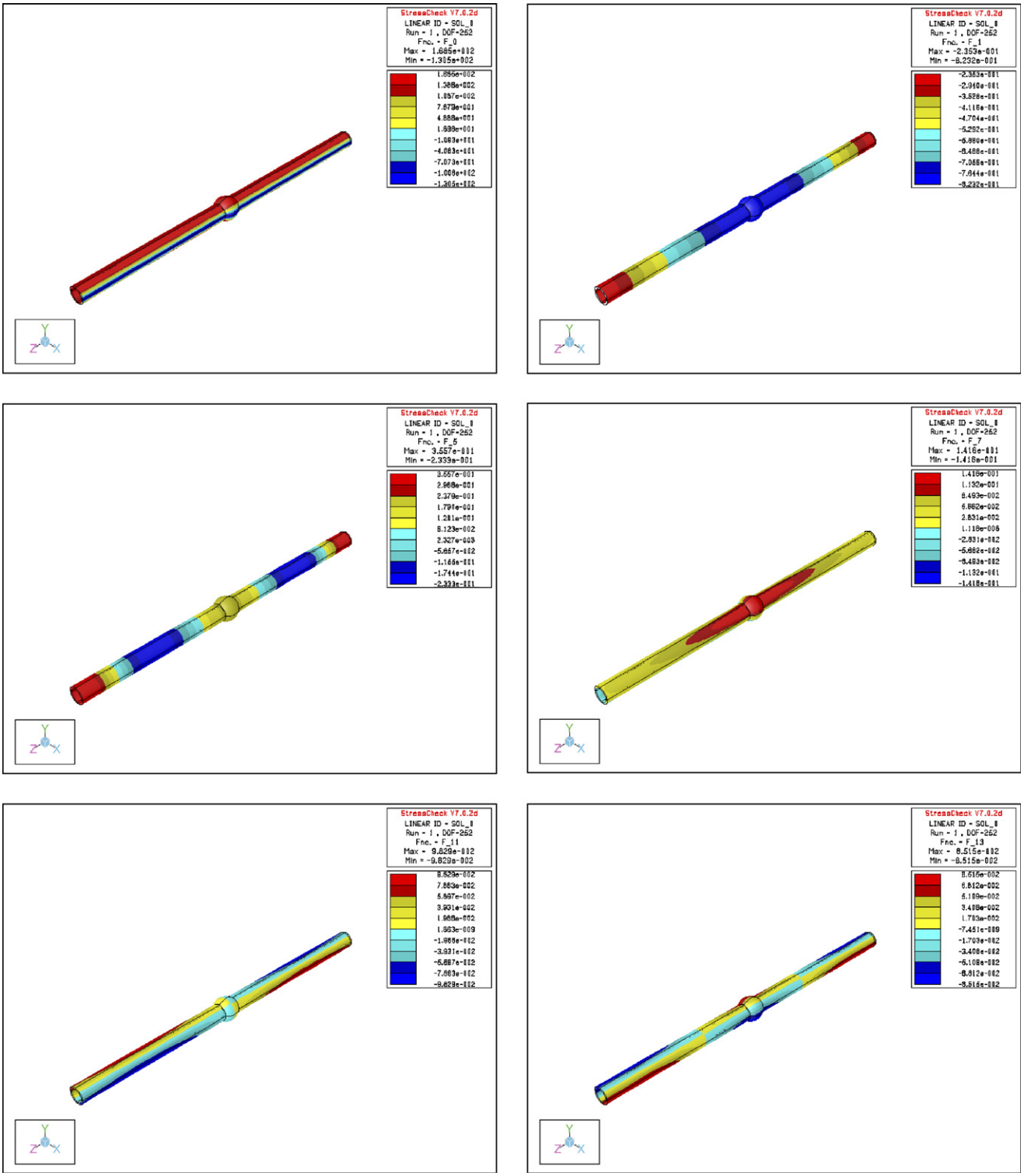

Fig. 5. Case I: Typical $(\mathscr{P}g)_k$ for $p_0 = 18$, $p_z = 6$.

example illustrates the benefits of using the Karhunen–Loéve expansion for random processes, where in this case only 20 deterministic problems had to be solved, instead of the large number of samples that Monte-Carlo *before* K–L would require (using Markov Chain Monte-Carlo, for example).

7.2. Case II: Random Young's modulus for 4140 steel

Consider the straight pipe (now without the spherical added mass, shown in Fig. 1C) in the flow field, and assume it is made of a 4140 steel cold finished according to ASTM A331 described in [16]. Here the cylinder with an inner

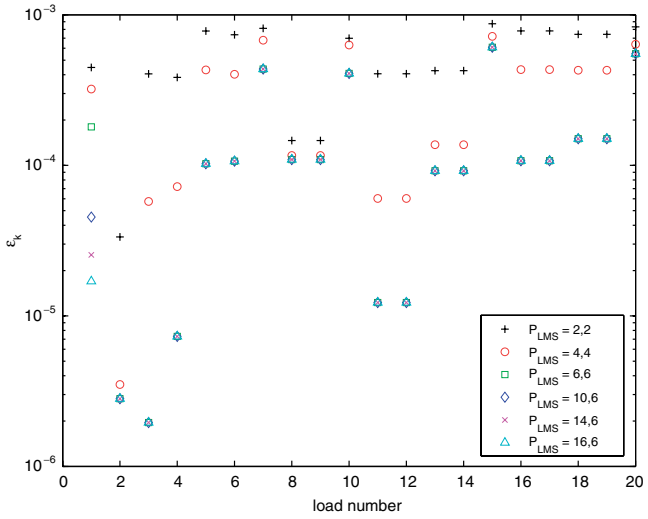

Fig. 6. Case I: LMS errors for each of 20 load functions, at various P_{LMS}. The notation $P_{\mathrm{LMS}} = 2,2$, for example, is used for the LMS approximation $(\mathscr{P}g)_k = \sum_{i=0,j=0}^{2,2} a_{ij}^k h_i(\theta) z^j$ in (64).

diameter of 0.4 m is used. As previously stated, we model the Young's modulus as a uniformly distributed random variable with mean of 212.74 GPa and standard deviation 7.26 GPa. We note that the method can be used for any arbitrary PDF with an appropriate choice of orthogonal polynomial basis with the correct weighting function. Thus, with a sufficient number of samples of experimental data, this example could be repeated using a statistical estimation of the PDF and corresponding polynomial basis. If we take ξ to be the standard uniform random variable on $[-1,1]$ with mean 0 and variance 1/3, we may write $E = 212.74 + 7.26\sqrt{3}\xi$ [GPa]. Legendre-chaos was used in the stochastic analysis since the orthogonality weight corresponds to the PDF. We note that the formulation and algorithms in Section 5.2 accommodates a general form of E as a spatially varying random process, but here we have chosen a simplistic case in order to verify the method.

The pipe is loaded by the realistic mean pressure field as reported in the experiment on the cylinder in flow [15],

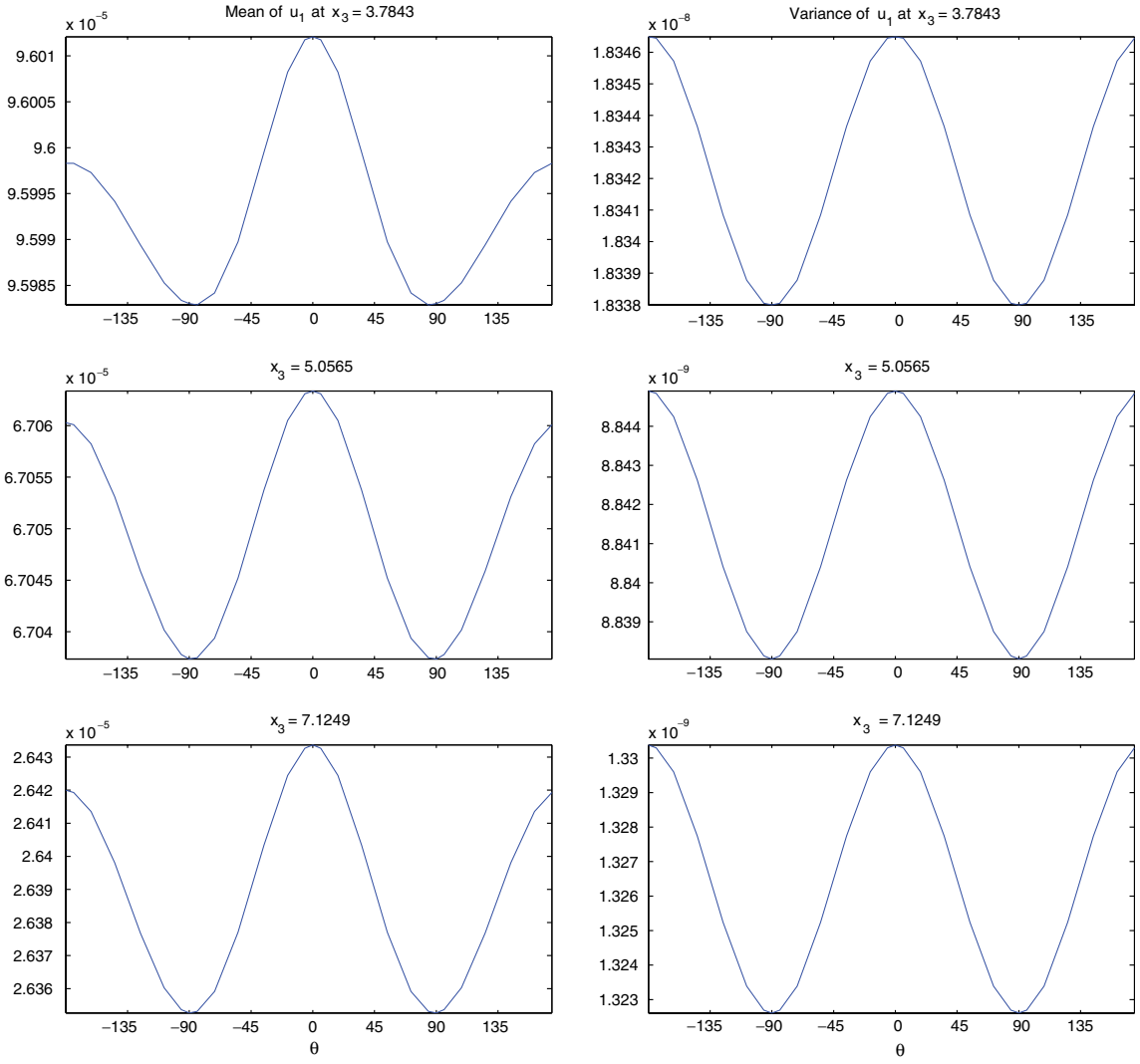

Fig. 7. Case I: u_1 profiles on the surface at $x_3 = 3.78$, 5.06, 7.13 for the finer mesh (see Fig. 1) with $P_{\mathrm{FEM}} = 8$. Mean (left) and variance (right).

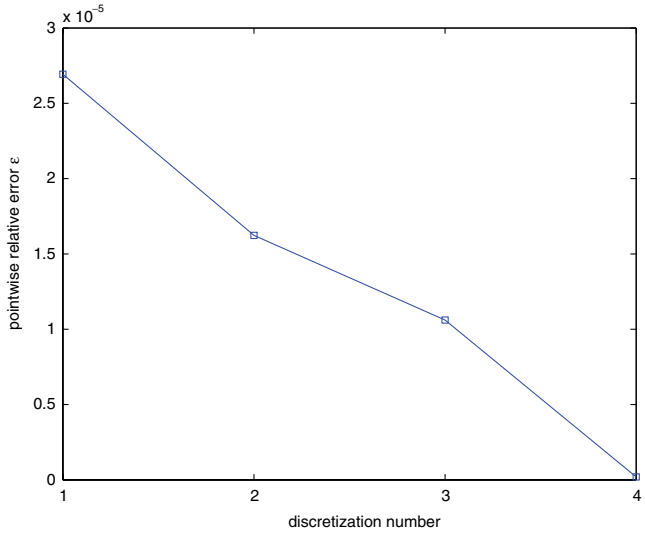

Fig. 8. Case I: Pointwise relative error in the variance of u_1 between discretizations $1,2,3$ (corresponding to $P_{\mathrm{FEM}} = 5,6,7$ on the coarse mesh) and discretization 4 ($P_{\mathrm{FEM}} = 7$ on the finer mesh), as compared to results at $P_{\mathrm{FEM}} = 8$ on the refined mesh.

according to (13). We perform a gPC analysis with gPC orders $N_{\mathrm{gpc}} = 2,4,6,8$ and finite element order $P_{\mathrm{FEM}} = 8$. Figs. 9 and 10 show the mean and variance of the displacement u_1 at three different x_3 locations obtained for a linear elastic analysis.

7.2.1. Convergence

We investigate the behavior of the numerical scheme by evaluating the relative convergence of results as the gPC order N_{gpc} is increased. The errors in variance of u_1 displacement between results from runs at $N_{\mathrm{gpc}} = 8$ and $N_{\mathrm{gpc}} = 1,2,4,6$ are calculated according to (67) and plotted in Fig. 11. The solution at $N_{\mathrm{gpc}} = 8$ is taken to be the reference solution in the error definition. The convergence observed is exponential. Numerical experiments were also performed at $N_{\mathrm{gpc}} > 8$, but yielded results virtually identical to those at $N_{\mathrm{gpc}} = 8$. As we can see, with a realistic level of uncertainty in the Young's modulus we achieve very good results even with low-order polynomial chaos.

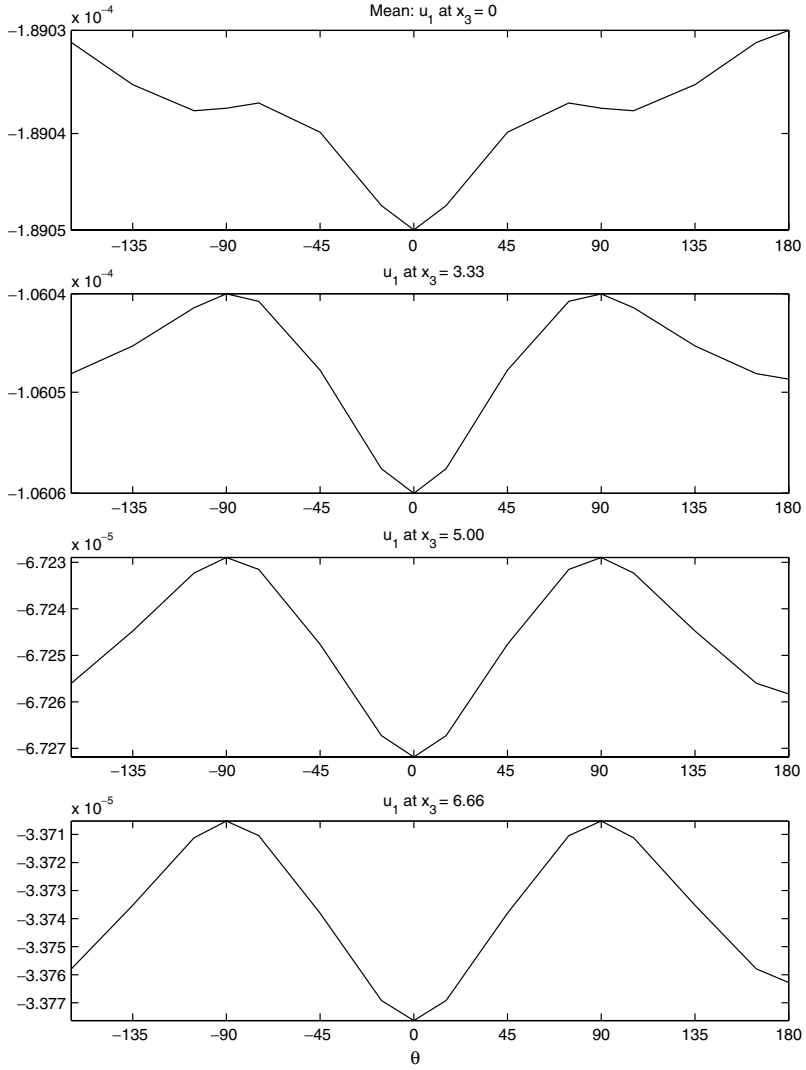

Fig. 9. Case II: Mean of u_1 at the outer surface at $x_3 = 0$, 3.33, 5.00, 6.66 along the pipe obtained by gPC of order $N_{\mathrm{gpc}} = 8$ and $P_{\mathrm{FEM}} = 8$.

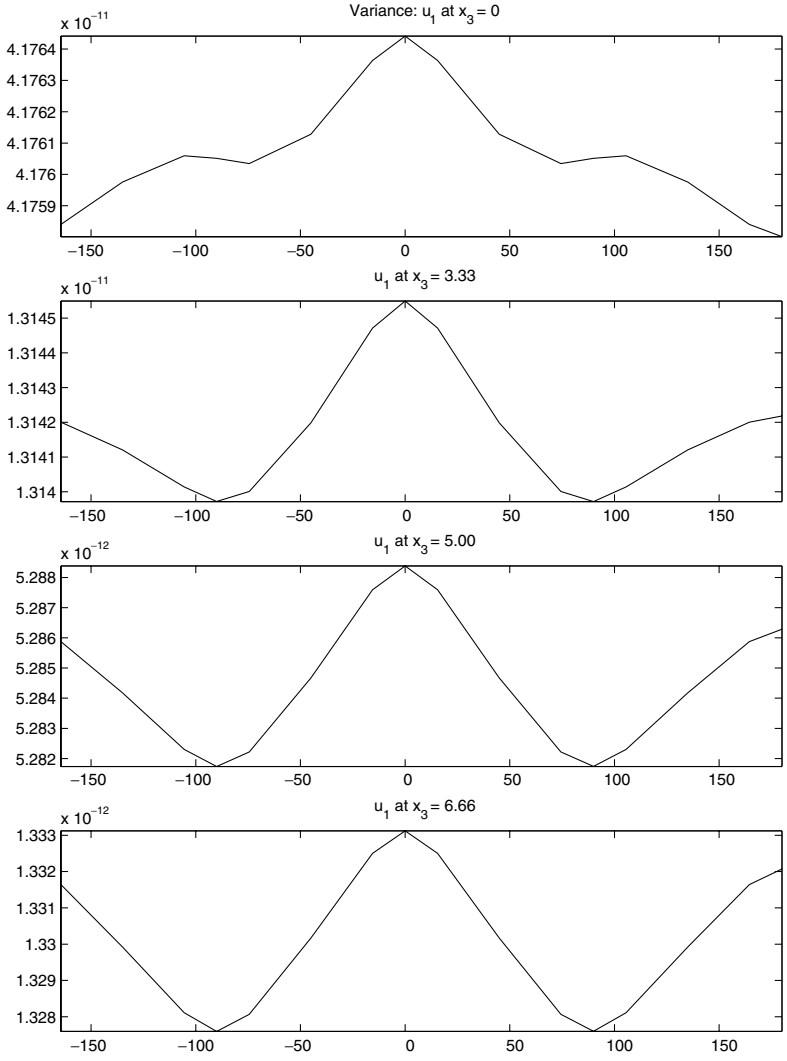

Fig. 10. Case II: Variance of u_1 at the outer surface at $x_3 = 0$, 3.33, 5.00, 6.67 along the pipe obtained by gPC with $N_{\text{gpc}} = 8$.

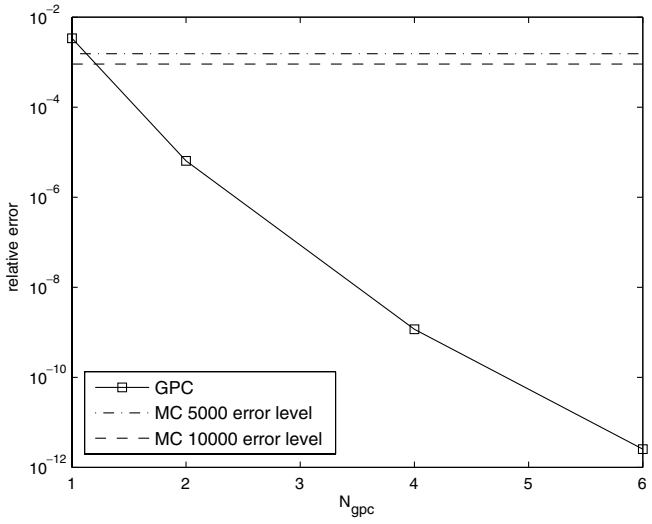

Fig. 11. Case II: Relative error ϵ between gPC of orders $N_{\text{gpc}} = 1, 2, 4, 6$ and $N_{\text{gpc}} = 8$. The horizontal dotted lines correspond to Monte-Carlo results.

7.2.2. Comparison with Monte-Carlo simulations

A standard Monte-Carlo simulation is performed and the mean and variance of displacements is compared with the gPC results. For the noise level in this problem the computational cost of a Monte-Carlo simulation accurate enough to obtain a 'reference' solution is extremely high. Thus, we once again use the gPC solution of order 8 as the reference solution. In Fig. 11 the relative error level in variance for MC with 5000 and 10,000 samples is plotted over the error plot for gPC convergence. Using the same error definition in (67), we find that after 10,000 iterations, the integrated relative error (for u_1 displacement) between Monte-Carlo and the reference solution is $9.1 \times (10)^{-4}$ in the mean and $9.2 \times (10)^{-3}$ in the variance. From Fig. 11 we note that using gPC order $N_{\text{gpc}} = 2$ in this case would be sufficient to achieve the same or better accuracy. Since the Gauss–Seidel procedure takes an average of 3 iterations to converge, for this error tolerance we achieve a speed-up ratio of the order 10^3 from MC to gPC. In Fig. 12 we plot the variance in u_1 obtained from MC with 10,000 samples.

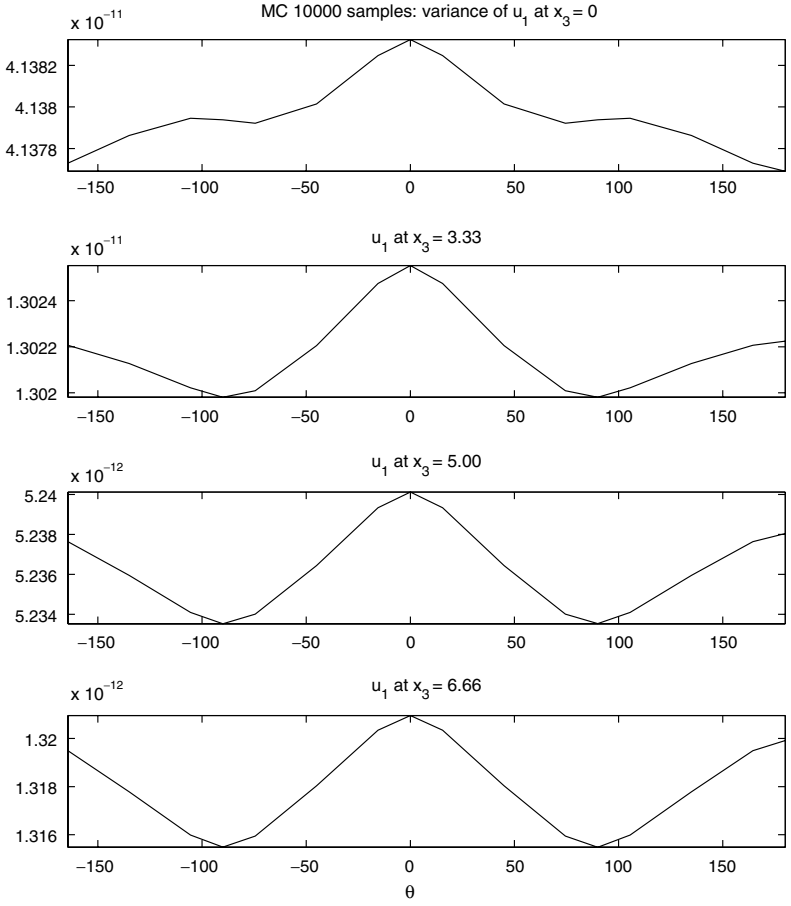

Fig. 12. Case II: Variance of u_1 at $x_3 = 0.0$, 3.33, 5.00, 6.66 obtained using Monte-Carlo with 10,000 samples.

Note that this figure should be compared to Fig. 10 to see the difference between the reference gPC solution and the MC solution with 10,000 samples. However, because of the scale of the solution and the difference in values they cannot be put on the same plot.

7.3. Case III

We solve these problems on the model shown in Fig. 1C with an inner diameter of 0.48 m. The deterministic boundary conditions are given by (13) but multiplied by a factor of 10^3 in order to amplify the difference between linear/nonlinear elasticity analyses. In the present example we aim to show that the stochastic collocation solution converges to the Monte-Carlo solution. Since the computational cost of doing MC simulation for nonlinear elasticity is high, we choose a low amplitude random input. The Young's modulus is defined $E = 212.74 + \xi$, where ξ is a random variable distributed uniformly on $[-1, 1]$. The collocation points for this one-dimensional space are chosen to be Chebyshev–Gauss–Lobatto nodes (also called Chebyshev extrema). In Figs. 13 and 14 we present results from the linear and nonlinear analyses, respectively. In these figures we plot the collocation estimates of the first and second moments as well as Monte-Carlo simulation estimates from 2000 samples. These estimates are plotted on the circumference of a slice of the cylinder taken from its free end at $x_3 = 0.0001$. The collocation grid points used in these plots consist of 80 Chebyshev extrema. The agreement between MC and stochastic collocation is very good in the eyeball norm. We quantify the convergence in the next plot, Fig. 15, where we show the convergence of collocation second moment estimate to the MC solution with increasing grid refinement in the random space, which corresponds to increasing the number of grid points on $[-1, 1]$. The error between two solutions u and v on a particular slice with N points is defined to be

$$\epsilon_{\text{slice}} = \frac{\sum_{i=1}^{N} |u(\boldsymbol{x}^i) - v(\boldsymbol{x}^i)|}{N}. \tag{68}$$

In the present examples, the solution is calculated on $N = 32$ points at each slice in the x_3 direction. Monte-Carlo with a very large number of samples is computationally prohibitive in this case, since each nonlinear elasticity-solve with the p-FEM code is costly. Thus, we compare our collocation solutions with MC at 2000 samples. Note that the error does not decay to zero as the stochastic collocation grid refinement increases – this is due to the fact that other errors from the MC estimates as well as the spatial FEM error limit the accuracy, thus dominating the error at these

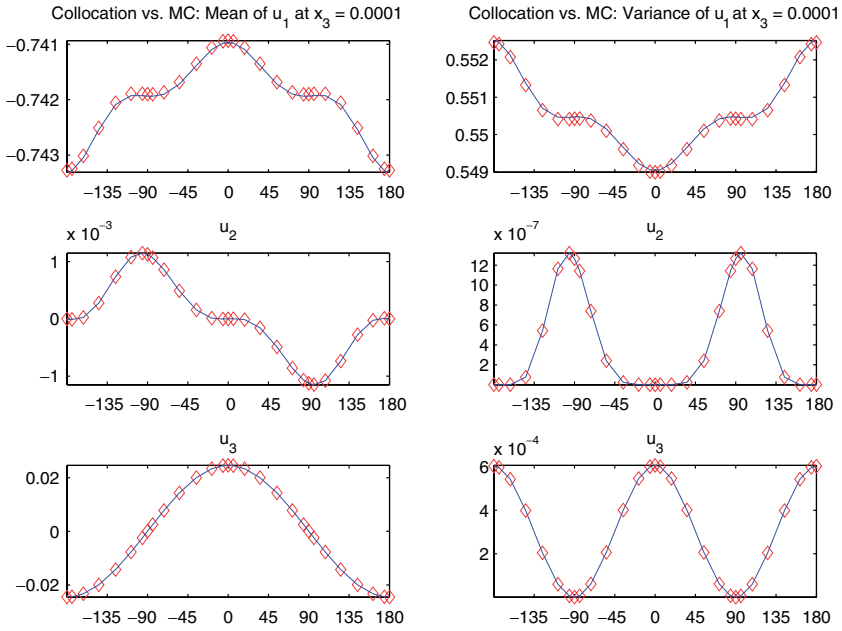

Fig. 13. Case III: Linear elasticity. First and second moments of u_1. Line: MC, diamond: 80-pt collocation.

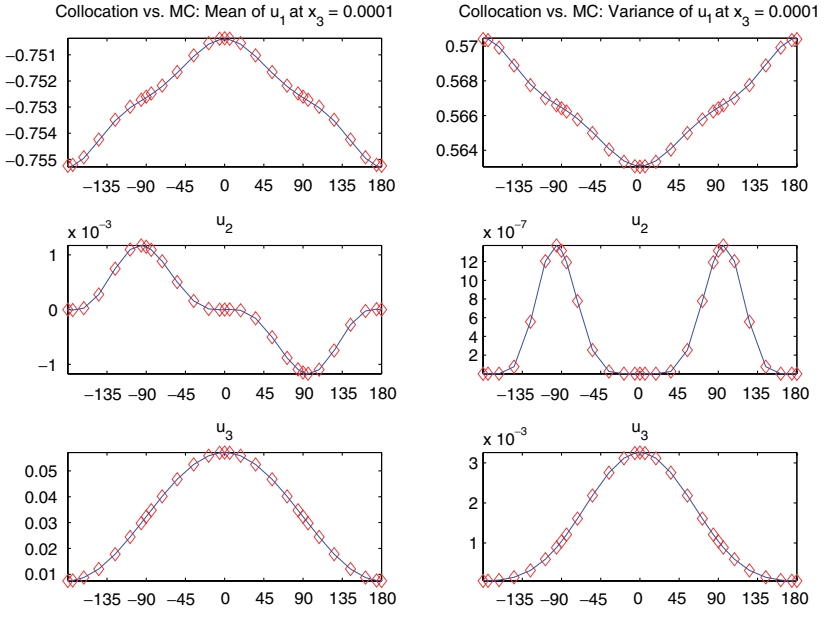

Fig. 14. Case III: Nonlinear elasticity. First and second moments of u_1. Line: MC, diamond: 80-pt collocation.

lower levels. We can see that beyond a level of 80 collocation points, the error of MC at 2000 samples exceeds the error of collocation.

In addition, note that performing stochastic collocation with just 20 grid points we obtain an error of less than 0.1% of the MC estimate.

The difference in PDFs of the solutions of linear and nonlinear elastic analyses is highlighted in Figs. 13 and 14. Whenever the magnitudes of the mean and variance are significantly large, their profiles differ significantly between the linear and nonlinear cases. Note that the probability density functions of the input material properties are identical. However, since the problem exhibits a *nonlinearity in random space*, the PDFs of the systems' solutions are markedly different, exhibiting differences in both mean and variance.

In Fig. 16 we show the consistency of the method by plotting the exponential convergence of the collocation solution to the 160-pt collocation solution with increasing grid refinement.

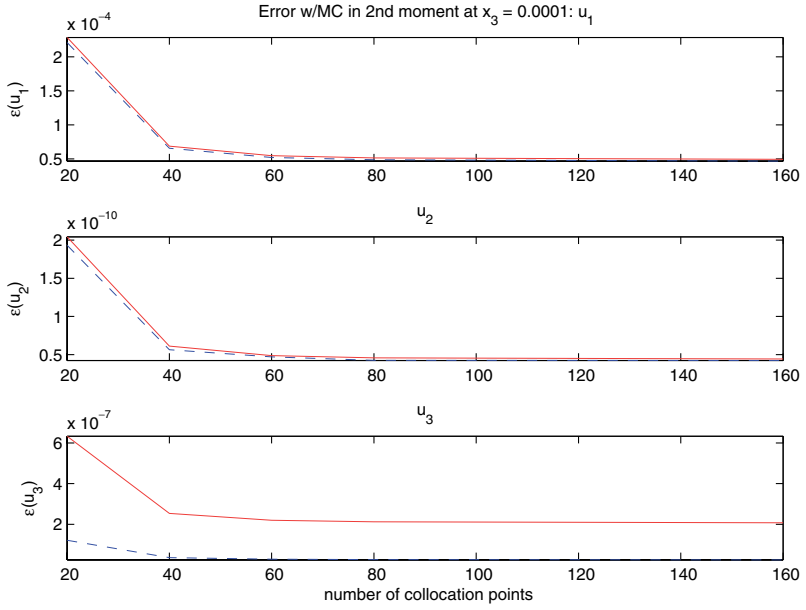

Fig. 15. Case III: Error in u_1, u_2, and u_3 between collocation with MC 2000. Dashed: linear elasticity, solid: nonlinear elasticity.

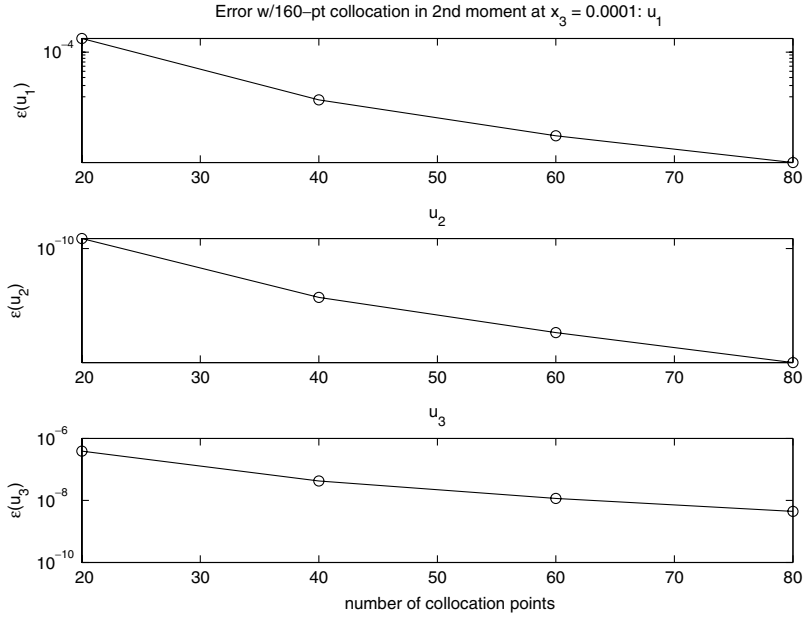

Fig. 16. Case III: Error of collocation compared to 160-pt collocation. Nonlinear elasticity.

7.3.1. A comparison between gPC and stochastic collocation

One may note that both Case II and Case III address a linear elasticity problem with stochastic Young's modulus. In Case II an iterative algorithm to solve the coupled system was used to speed-up the gPC method. Here in Case III, the stochastic collocation method is performed on a similar problem with a smaller noise level. (As mentioned above, this choice was made so that accurate Monte-Carlo simulations would be computationally feasible). An interesting question arises: if gPC and stochastic collocation are performed on the same problem, which will be more efficient? In Table 1 we compare the computational work required by each method in order to reach a desired level

Table 1
Number of deterministic solves required by gPC and stochastic collocation to achieve different error tolerance levels

Error	gPC	Stochastic collocation
10^{-3}	3	3
10^{-5}	6	4
10^{-7}	9	5
10^{-8}	12	6

of accuracy in variance. The error is defined as in (67), and the amount of work is measured in terms of the number of 'deterministic solves' needed. In the gPC method, the order of the polynomial expansion is increased to achieve the accuracy level. Analogously, for the stochastic collocation method the number of collocation points is increased.

From the table, it can be seen that the two methods are comparable in efficiency for this linear elasticity problem with a one-dimensional random input.

7.4. Case IV

We solve these problems on the model shown in Fig. 1A (inner diameter of 0.48 m) with deterministic Young's modulus of 212.74 GPa. In these examples we take $\alpha = 0.05$ and β set at approximately 3% of the mean forcing (see Section 5.5). For the mean forcing, the expression in (13) is multiplied by a factor of 10^3 in order to highlight significant differences between the linear and nonlinear elasticity solutions. The computationally expensive MC validation is not performed for this example, since the method was validated in the simpler test problem of Case III. Instead, we investigate the convergence of the collocation solution as the collocation grid becomes more refined. In Fig. 17 we plot the mean and variance of the linear and nonlinear solutions on three slices of the cylinder, using the 65-pt collocation grid shown in Fig. 18b. Once again we see that the PDF of the solution changes due to a problem nonlinearity in random space. The 13-pt collocation on the grid in Fig. 18a was also performed for the same random input, and the error between solutions at these two collocation levels is shown in Table 2 for linear and nonlinear elasticity. The error between two functions u and v for N data points on the cylinder is defined as in (68).

Thus, we note that the difference between the 13 and 65-pt collocation solutions is less than 0.01% of the estimate at 65-pts. The errors in the linear and nonlinear analyses are comparable, showing that the stochastic collocation method performs well for both types of problems. In Fig. 18b we may see that the full collocation grid corresponding to the 13-pt sparse grid is completely incorporated into the 65-pt grid. Thus, the difference between the 13-pt sparse grid and its associated full grid of the same order is bounded above by the errors in Tables 1 and 2. The accuracy we 'lose' by using the sparse grid is small. Fig. 18c shows the 165-pt full grid with the same order as the 65-pt sparse grid, and Fig. 18d shows the magnitude of the nonlinear elasticity solution u_1 at an example point $(-0.25, 0, 0)$ for each of the 65 collocation points. The vertical axis represents ξ_1, the multiplicative noise dimension, and the horizontal axis represents ξ_2. We note that the variation in the solution is almost negligible in the ξ_2 direction but noticeable in the ξ_1 direction, reflecting the nature of the random input.

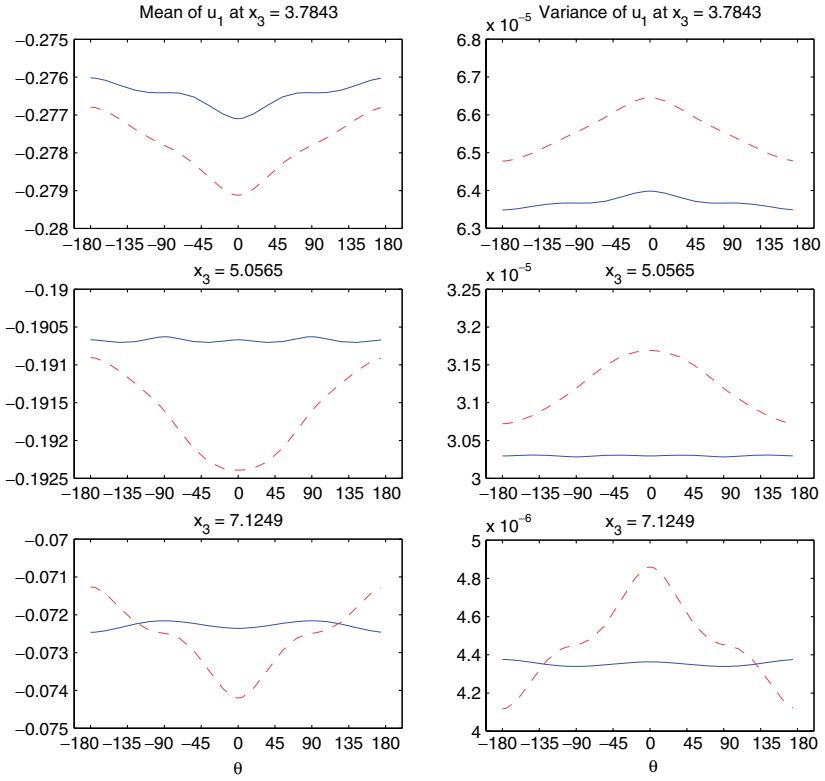

Fig. 17. First and second moments of u_1 at several locations along the rise, using 65-pt sparse grid collocation. Solid: linear elasticity, dashed: nonlinear elasticity.

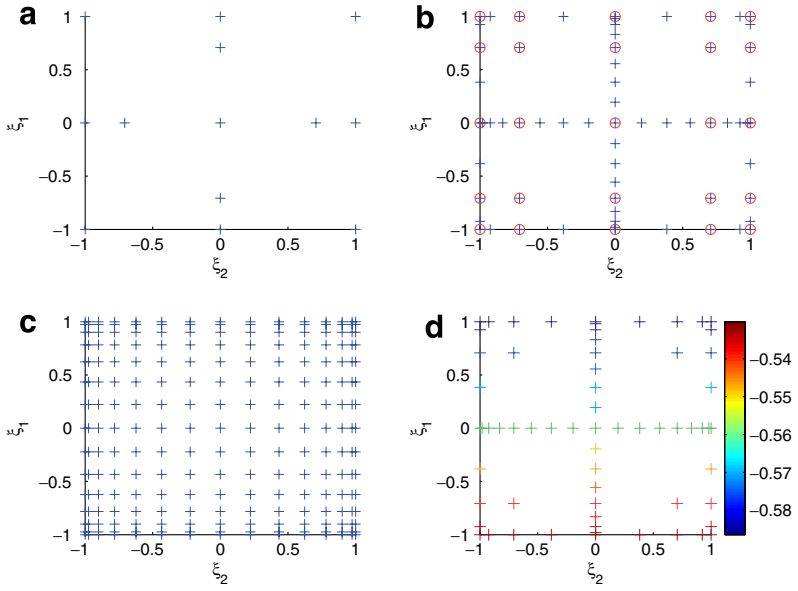

Fig. 18. (a) 13-pt sparse grid, (b) 65-pt sparse grid (crosses), 25-pt full grid (circles) (c) 156-pt full grid, (d) NL elasticity u_1 solution at point $(-0.25, 0, 0)$ on a 65-pt sparse grid.

Table 2
Error between 13 and 65 point collocation results

	Linear elasticity		Nonlinear elasticity	
	Mean	Variance	Mean	Variance
u_1	$9.5e^{-9}$	$1.13e^{-9}$	$2.25e^{-8}$	$1.12e^{-9}$
u_2	$8.70e^{-9}$	$1.05e^{-13}$	$4.36e^{-8}$	$8.05e^{-13}$
u_3	$6.48e^{-10}$	$2.02e^{-12}$	$2.42e^{-9}$	$5.04e^{-12}$

8. Summary

The gPC and stochastic collocation approaches for reducing the 3-D elastic problems with stochastic inputs to a high-dimensional deterministic system of PDEs were formulated and investigated numerically using p-FEMs for the spatial discretization. Three-dimensional riser-like structures undergoing linear and geometrically nonlinear elastic deformations due to stochastic pressure loading were considered as well as a riser with stochastic Young's modulus (with uncertainty data taken from experimental results documented in [16]) under deterministic fluid pressure. We note that realistic risers may be much longer than the models we have addressed, and also that the loads encountered for cylinders undergoing vortex-induced vibrations (VIV) may be very different than those for stationary cylinders. However, for such cases the data sets analogous to the set in [15] are difficult to find. It has been demonstrated that the gPC method for linear elasticity systems provide accurate and efficient results at a speed factor of two and three orders of magnitude compared to traditional Monte-Carlo simulations. Furthermore, these methods can be implemented by using standard deterministic FE codes as black boxes. Both uncertain traction loadings and uncertain material properties were considered, leading to additive and multiplicative uncertainties, and an efficient algorithm for solving the gPC system for the multiplicative uncertainty case was presented. The stochastic collocation method was demonstrated for both linear and nonlinear elasticity problems with multiplicative and additive uncertainty. The simplicity of the method as compared to the gPC method was exhibited, and although it was computationally difficult to perform accurate Monte-Carlo simulations on these 3D elasticity problems, a large speed-up ratio was observed in problems with nonlinearities in random space and low random dimension. For the simple linear elasticity problem with stochastic pressure loading, the stochastic collocation and gPC methods were shown to be comparable in efficiency.

The present study can be generalized to additive and multiplicative uncertainty for plasticity problems, in which the constitutive equations have a much wider stochastic variability as shown by [4]. This generalization will enable stochastic analyses for problems that are computationally prohibited if MC simulations are required.

Acknowledgements

The authors gratefully acknowledge the support of this work by the Office of Naval Research (Ocean Engineering and Marine Systems), and the United States-Israel Binational Science Foundation. The computations were performed on DoD's supercomputing center (NAVO, ARSC and ARL) under a HPCMP grant.

The first author would like to acknowledge the support of the US Department of Energy Computational Science Graduate Fellowship under grant number DE-FG02-97ER25308 and the Krell Institute.

References

[1] T. Soong, M. Grigoriu, Random Vibration of Mechanical and Structural Systems, Prentice-Hall, Englewood Cliffs, NJ, 1993.

[2] R.G. Ghanem, R.M. Kruger, Numerical solution of spectral stochastic finite element systems, Comput. Methods Appl. Mech. Engrg. 129 (1996) 289–303.

[3] G. Stefanou, M. Papadrakakis, Stochastic finite element analysis of shells with combined random material and geometric properties, Comput. Methods Appl. Mech. Engrg. 193 (2004) 139–160.

[4] M. Anders, M. Hori, Three-dimensional stochastic finite element method for elasto-plastic bodies, Int. J. Numer. Methods Engrg. 51 (2001) 449–478.

[5] D. Xiu, G. Karniadakis, The Wiener-Askey polynomial chaos for stochastic differential equations, SIAM J. Sci. Comput. 24 (2) (2002) 619–644.

[6] N. Wiener, The homogeneous chaos, Am. J. Math. 60 (1938) 897–936.

[7] R. Ghanem, P. Spanos, Stochastic Finite Elements: A Spectral Approach, Springer, New York, 1991.

[8] P. Frauenfelder, C. Schwab, R.A. Todor, Finite elements for elliptic problems with stochastic coefficients, Comput. Methods Appl. Mech. Engrg. 194 (2005) 205–228.

[9] I. Babuska, R. Tempone, G.E. Zouraris, Solving elliptic boundary value problems with uncertain coefficients by the finite element method: the stochastic formulation, Comput. Methods Appl. Mech. Engrg. 194 (12–16) (2005) 1251–1294.

[10] H.G. Matthies, A. Keese, Galerkin methods for linear and nonlinear elliptic stochastic partial differential equations, Comput. Methods Appl. Mech. Engrg. 194 (2005) 1295–1331.

[11] D. Xiu, J. Hesthaven, High-order collocation methods for differential equations with random inputs, SIAM J. Sci. Comput. 27 (2005) 1118–1139.

[12] I.S. Sokolnikoff, Mathematical Theory of Elasticity, McGraw-Hill, New York, 1956.

[13] B.A. Szabó, I. Babuška, Finite Element Analysis, John Wiley & Sons, New York, 1991.

[14] A. Noel, B. Szabó, Formulation of geometrically non-linear problems in the spatial reference frame, Int. J. Numer. Methods Engrg. 40 (1997) 1263–1280.

[15] C. Norberg, Pressure forces on a cylinder in cross flow, IUTAM Symposium on Bluff-Body Wakes, Dynamics and Instabilities, 7–11 September 1992.

[16] M. Radovic, E. Lara-Curzion, L. Riester, Comparison of different experimental techniques for determination of elastic properties of solids, Mater. Sci. Engrg. A 368 (2004) 56–70.

[17] E. Jaynes, Information Theory and Statistical Mechanics, Phys. Rev. 106 (1957) 620–630.

[18] E. Jaynes, Information Theory and Statistical Mechanics, II, Phys. Rev. 108 (1957) 171–190.

[19] R.H. Cameron, W.T. Martin, The orthogonal development of nonlinear functionals in series of Fourier–Hermite functionals, Ann. Math. 48 (1947) 385.

[20] X. Wan, G.E. Karniadakis, Multi-element generalized polynomial chaos for arbitrary probability measures, SIAM J. Sci. Comput. 28 (3) (2006) 901–928.

[21] M. Loéve, Probability Theory II, Springer, New York, 1997.

[22] I. Babuska, F. Nobile, R. Tempone, A stochastic collocation method for elliptic partial differential equations with random input data, SIAM J. Numer. Anal., submitted for publication.

[23] B. Oksendal, Stochastic Differential Equations, fifth ed., Springer, 1998.

[24] X. Wan, G.E. Karniadakis, An adaptive multi-element generalized polynomial chaos method for stochastic differential equations, J. Comput. Phys. 209 (2) (2005) 617–642.

[25] O.P.L. Maitre, H.N. Njam, R.G. Ghanem, O.M. Knio, Multi-resolution analysis of Wiener-type uncertainty propagation schemes, J. Comput. Phys. 197 (2004) 502–531.

[26] M. Tatang, G. McRae, Direct treatment of uncertainty in models of reaction and transport, MIT Technical Reports.

[27] A. Keese, H. Matthies, Numerical methods and Smolyak quadrature for nonlinear partial differential equations, Informatikbericht 2003-5, Technische Universitat Braunschweig.

[28] S. Smolyak, Quadrature and interpolation formulas for tensor products of certain classes of functions, Sov. Math. Dokl. 4 (1963) 240–243.

[29] E. Novak, K. Ritter, High dimension integration of smooth functions over cubes, Numer. Math. 75 (1996) 79–97.

[30] D. Lucor, C.-H. Su, G. Karniadakis, Covariance kernal representations of multidimensional second-order stochastic processes, J. Comput. Phys. 217 (1) (2006) 82–99.

[31] R. Ghanem, A. Doostan, On the construction and analysis of stochastic models: characterization and propagation of the errors associated with limited data, J. Comput. Phys. 217 (2006) 63–81.